REVIEWS OF TOPICAL PROBLEMS

Coherent four-wave mixing in excited and ionized gas media: four-photon spectrochronography, ellipsometry, and nonlinear-optical imaging of atoms and ions

A M Zheltikov, N I Koroteev

Contents

Abstract. A review of the main directions of development, the most promising new techniques, and urgent applications of coherent four-photon methods of investigation of excited and ionized gas media is presented. It is demonstrated that the methods of coherent four-wave mixing (FWM) provide important spectrochronographic information on atoms and ions, allow selective studies of separate components of nonstationary gas and plasma systems with a complex composition using polarization-sensitive four-photon spectroscopy and coherent ellipsometry, and permit nonlinear-optical imaging of the spatial distribution of atoms and ions in excited gases and plasmas.

A M Zheltikov, N I Koroteev
M V Lomonosov Moscow State University, Physics Department,
International Laser Center,
Vorob'evy Gory, 119899 Moscow, Russian Federation
Tel. (7-095) 939 39 59
Fax (7-095) 939 31 13
E-mail: zheltikov@nls1.ilc.msu.su

1. Introduction

The nonlinear optics of excited and ionized gas media is a rapidly developing area of modern physical research. The growing interest in the investigation of nonlinear-optical interactions in gases is associated with both the necessity of developing local nonperturbing methods of diagnostics of fast processes in excited gas media and plasmas and the possibility of using the nonlinearities of such media for the generation of coherent short-wavelength radiation by means of optical frequency conversion. The coherently scattered signal in the nonlinear spectroscopy of gas media [1 – 4] carries information concerning the chemical composition, populations of quantum levels, the temperature, the velocity distributions and other parameters of atoms and molecules. One of the main advantages of these methods is associated with the fact that they allow the probing of objects characterized by a high level of intrinsic emission, including flames [5 – 8], highly excited gases [9, 10], and plasmas of electric [11 – 14] and optical [15 – 18] discharges. In particular, the methods of coherent four-photon spectroscopy have received wide application in combustion diagnostics in automotive and rocket engines [19, 20], the investigation of chemical reac-

tions involved in chemical vapor deposition [21], studies of active media of gas-discharge lasers [22], and ecological applications [23].

Although coherent four-wave mixing (FWM) has been successfully applied to the investigation of molecular and condensed media for quite a long period of time, recent experiments have demonstrated that the use of this technique for the diagnostics of plasmas and excited gases [14, 22, 24 – 26] requires certain modifications in the methodology of measurements and more in-depth investigations in the theory of coherent FWM. Specifically, recent experiments have revealed the high efficiency of nonlinear-optical interactions of intense laser radiation with excited gases and plasma. It is often difficult to apply numerous thoroughly developed methods of molecular four-photon spectroscopy in such media because of the high temperatures of the gas, when one is mainly dealing with atomic or ionic species. Therefore, we encounter the necessity of developing diagnostic methods for the atomic and ionic components of excited gases. In particular, as demonstrated in Refs [22, 24], FWM spectroscopy with hyper-Raman resonances is an efficient tool for the investigation of the atomic and ionic components of gas-discharge and laser-produced plasmas. Due to its high spatial, temporal, and spectral resolutions and the broad variety of polarization techniques, FWM spectroscopy with Raman and hyper-Raman resonances makes it possible to obtain valuable information about plasma parameters.

Excited states of atoms and ions play an important role in resonant and quasi-resonant interaction of laser radiation with gases and plasmas. Therefore, experimental investigation of temporal dynamics and spatial distributions of excited atoms and ions in gases and plasmas is important for understanding the specific features of nonlinear-optical interactions in such media. It should be mentioned that nonlinear-optical processes accompanying the interaction of laser radiation with excited atomic gases have been studied rather intensively and are widely employed at the present time for optical frequency conversion and spectroscopic applications. The results of early experimental and theoretical studies in this area were systematically analyzed and generalized by Butylkin et al. [27]. A comprehensive theoretical analysis of such phenomena and a detailed discussion of the experimental data obtained in this direction up to the middle 1980s are presented in monographs [2, 28 – 30].

The development of methods for the diagnostics of nonstationary and spatially nonuniform plasma media, including plasmas of optical breakdown and electric discharge, is currently one of the most important (and challenging) problems of the investigation of nonlinear-optical interactions in excited and ionized gas media. The solution of this problem requires a combination of experimental techniques simultaneously possessing high spatial and temporal resolutions and allowing the main parameters of a gas medium to be measured with a minimum time of averaging. The material of this review indicates, in our opinion, that the variety of coherent FWM methods now accumulated, including coherent spectrochronography [31] and ellipsometry [3, 32, 33], as well as nonlinear-optical imaging of spatial distributions of physical parameters of gas media [34, 35], provides an opportunity to solve these and some similar difficult experimental problems.

The nonlinear-optical properties of laser-produced plasmas are currently actively investigated by many research groups in connection with the possibility of efficient genera-

tion of coherent short-wavelength radiation in such media [36 – 49]. The use of a low-temperature laser-produced plasma as a nonlinear medium makes it possible to achieve a sufficiently high efficiency of conversion of pulsed Nd:YAG-laser radiation into the third harmonic [36, 37]. In particular, recent experiments [45 – 48] demonstrate that the plasma of optical breakdown in gases is an efficient source of coherent third-harmonic emission in the case when high-repetition-rate (1 kHz) femtosecond laser pulses with a moderate intensity (less than or on the order of 10^{15} W cm^{-2}) are used. Such applications of laser-produced plasmas, as well as many other applications of excited and ionized media considered below, employ a considerable (by several orders of magnitude) increase in nonlinear-optical susceptibilities of atomic and plasma media that accompanies the growth in the excitation degree of such media. Due to this effect, even relatively low densities of excited atoms and ions may provide coherent resonance and quasi-resonance FWM signals with a sufficiently high intensity, which can be easily detected against the background of incoherent emission and masking coherent processes involving ground-state atoms.

We should note that the increase in the nonlinear-optical susceptibility of an atomic system due to the population of excited states was predicted quite a long time ago [50]. Gladkov et al. [18, 51] have demonstrated that the quasi-resonant increase of the third-order nonlinear-optical susceptibility of excited atoms in an optical breakdown ensures coherent four-photon scattering with an efficiency sufficient for the reliable detection of the nonlinear-optical signal. Reviews [12, 17] were devoted to the analysis of early experiments in this direction and the discussion of possible applications of coherent anti-Stokes Raman scattering for the diagnostics of laser-produced and gas-discharge plasmas. Until recently, laser-produced plasma has not been a conventional object for coherent four-photon spectroscopy because of the considerable difficulties associated with intense plasma emission, a high nonresonance coherent background, as well as strong absorption and considerable phase-mismatch effects at certain stages of plasma expansion. Additional factors that drastically lower the accuracy of nonlinear-optical measurements in laser-produced plasmas are associated with inevitable fluctuations of plasma parameters from pulse to pulse and the complexity of FWM spectra, featuring a tremendous number of lines that are difficult to interpret and that often mask the spectral lines of interest [52].

Luckily, coherent four-photon spectroscopy provides us with a rich variety of tools to solve the problems listed above. In particular, the level of incoherent background can be considerably decreased by means of time gating and spatial filtering of the coherent FWM signal, while the noninformative coherent background can be suppressed with an appropriate choice of polarization conditions for the excitation and detection of coherent spectra.[1] Distortions in spectral and temporal dependences of the FWM signal due to phase mismatch and population variations can be eliminated with an adequate choice of delay times and intensities of probing laser pulses and with an optimization of the experimental geometry.

---

[1] The polarization technique, often referred to as holographic multidimensional spectroscopy (a review of numerous Lorentzian-line applications of this technique was given elsewhere [53]) provides an opportunity to resolve closely spaced and overlapping spectral lines related to different plasma species and to investigate these lines independently of each other.

As mentioned above, experimental investigation of the temporal dynamics and spatial distributions of atomic and ionic components of a laser-produced plasma is an important problem of laser-plasma diagnostics. The possibilities of different methods of laser spectroscopy for extracting the data concerning the spatial distribution of particles in excited gas media have been widely discussed in recent years. Along with the methods of emission spectroscopy and laser-induced fluorescence, coherent FWM schemes are finding increasing applications for this purpose, ensuring a high spatial and temporal resolutions and allowing a high contrast of the coherent signal with respect to the emission background to be achieved. Several attractive schemes for the two-dimensional imaging of spatial distributions of parameters of excited gases and plasmas can be implemented with the use of degenerate four-wave mixing (DFWM) and coherent anti-Stokes Raman scattering (CARS) (see Section 2.1).

The main goal of this review is to discuss the main directions of development, the most promising novel techniques, and urgent applications of coherent four-photon methods of investigation of excited and ionized gas media. We will consider spectrochronographic schemes of coherent FWM, which provide information concerning the time evolution of FWM spectra, determined by the kinetics of excitation and relaxation of atoms and ions in a nonstationary inhomogeneous plasma. We will analyze polarization-sensitive FWM schemes and methods of coherent ellipsometry, allowing selective investigation of separate components of nonstationary gas and plasma systems with a complex composition. We will also discuss in detail the methods that were recently proposed and that find rapidly growing applications for imaging spatial distributions of atoms and ions in excited gases and plasmas.

This review is organized in the following way. In Section 2, we briefly describe the main schemes of coherent FWM employed for the investigation of excited and ionized gases, such as degenerate four-wave mixing, FWM with Raman resonances, including CARS, FWM with hyper-Raman resonances, and third-harmonic generation. In Section 3, we provide the basic relations allowing a quantitative analysis of the influence of phase-matching and absorption effects on the parameters of the FWM signal and qualitatively consider how the regime of FWM changes depending on the relation between characteristic spatial scales of the problem. The main principles of the experimental technique and the measurement procedure are discussed in Section 4. In Section 5, we analyze the possibility of increasing the FWM efficiency in a laser-produced plasma due to intermediate hyper-Raman resonances. Spectrochronographic schemes of coherent FWM, considered in Section 6, provide an opportunity to investigate the relaxation kinetics of excited states of atoms and ions in a low-temperature plasma of optical breakdown and in a gas-discharge plasma. Issues related to polarization-sensitive four-photon spectroscopy and coherent ellipsometry of atoms and ions are discussed in Section 7. Section 8 is devoted to applications of coherent four-photon spectroscopy to the investigation of autoionizing states. In Section 9, we consider FWM schemes for imaging the spatial distributions of atomic and ionic plasma components. In particular, we will discuss how information about concentrations of resonant species can be extracted from the FWM signal averaged over a series of measurements under conditions when the concentrations of resonant species and the intensities of pumping laser beams are subject to fluctuations. We

will also consider FWM schemes for point-by-point mapping of atomic spatial distributions in a laser-produced plasma scanned with respect to probing laser beams, describe FWM methods for the reconstruction of spatial distributions of excited atoms in a laser-produced plasma line by line and slice by slice, and discuss the prospects of nonlinear-optical methods for the reconstruction of three-dimensional distributions of atoms and ions in a laser-produced plasma. The main conclusions of our analysis are briefly summarized in the final section of this review.
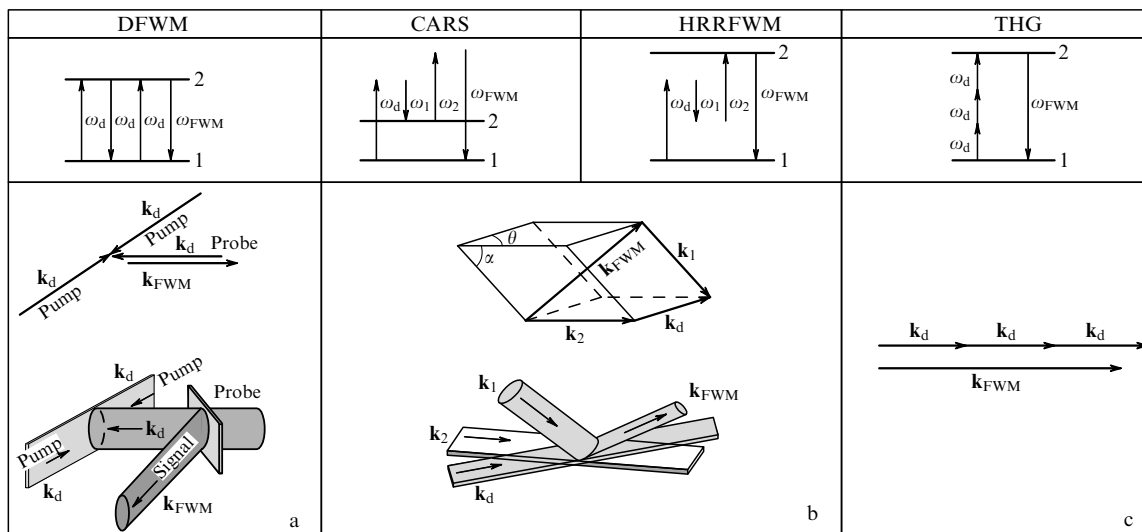
2. The main schemes of four-wave mixing in excited gases and plasmas

In this section, we will briefly consider the main schemes of coherent FWM employed for the investigation of excited and ionized gases, including degenerate four-wave mixing, FWM with Raman resonances, CARS included, hyper-Raman-resonance FWM (HRRFWM), and third-harmonic generation (THG). Below, we will describe the main features of these schemes and discuss their possibilities for plasma diagnostics.

2.1 Degenerate four-wave mixing
Degenerate four-wave mixing [54] (Fig. 1a), which was initially employed as a phase-conjugation scheme [55], has recently found extensive applications as a convenient and efficient method of spectroscopy (e.g., see Refs [2, 56 – 59]), which can provide, in particular, valuable information concerning the composition [58 – 61] and temperature [62 – 66] of gas media. Two salient modifications of DFWM with interaction in co- and counterpropagating beams are usually employed [2, 67]. The main advantages of the DFWM technique are associated with the fact that this approach requires only one laser source and allows the phase-matching conditions to be automatically satisfied regardless of the dispersion of the medium under study (see the wave-vector diagram in Fig. 1a). Broadband DFWM [68] makes it possible to measure the temperature of excited gases, including atomic gases [69], with a single laser pulse. Folded wide-beam DFWM schemes are employed in several convenient and elegant methods for two-dimensional imaging of spatial distributions of gas parameters [34, 70 – 72].

Significant progress in the development of DFWM as a method of diagnostics of excited atomic gases was achieved by Ewart and collaborators [56, 58], who observed and investigated DFWM involving excited states of sodium atoms and developed the DFWM technique for point-by-point mapping of the spatial distribution of sodium atoms in a flame. Subsequent studies in this direction demonstrated the possibility of applying coherent DFWM to wide beams for single-pulse two-dimensional imaging of spatial distributions of excited particles [34, 70] and temperature [71, 72] in gas media. Ljungberg and Axner [73, 74] have implemented two-step DFWM, which implies the detection of the DFWM signal from excited states selectively populated with an additional laser. In Ref. [74], this technique was applied to the investigation of excited gold atoms. Practically important aspects of DFWM with broadband pumping, including absorption effects and the dependence of the DFWM intensity on the interaction length, have been studied in Refs [75, 76]. A quantitative comparison of DFWM and laser-induced fluorescence (LIF) as techniques for NO_2 detection and imaging performed by Mann et al. [23] has shown that, under certain conditions, DFWM can be considered as a

DFWM	CARS	HRRFWM	THG

Figure 1. Main schemes of coherent FWM employed for the investigation of excited and ionized gases: (a) degenerate four-wave mixing; (b) FWM with Raman and hyper-Raman resonances, and (c) third-harmonic generation.

useful alternative to LIF. Konz et al. [77] have demonstrated the potential of folded two-photon-resonance DFWM [78] for the diagnostics of oxygen atoms in microwave-discharge plasmas. In certain cases, the use of this approach makes it possible to avoid distortions of the spectroscopic information provided by the signal of conventional DFWM with a one-photon resonance due to collisional quenching, absorption, and a high level of noise. A comprehensive analysis of various methodological problems of DFWM imaging, including diffraction effects, spatial resolution, and image referencing, has been provided by Ewart et al. [79].

We should note that, along with undeniable advantages, the DFWM method is characterized by several significant limitations. In particular, the laser radiation whose frequency in the DFWM scheme coincides with the frequency of the relevant molecular or atomic transition, may perturb resonance levels, thus distorting the spectroscopic information. The DFWM technique cannot be employed for the investigation of low-frequency transitions in molecular and atomic spectra, which usually provide important information on parameters of a gas medium. To remove these limitations, one has to employ frequency-nondegenerate coherent FWM. In the following subsections, we will consider the most widespread schemes of two- and three-color FWM.

2.2 Four-wave mixing with a Raman resonance
A four-photon process with a Raman resonance (in particular, CARS) is a classical scheme of nonlinear-optical spectroscopy of gases [80 – 82] (see the diagram at the left of Fig. 1b). Due to the high spatial, temporal, and spectral resolutions, the possibilities of studying highly luminous objects, and a rich variety of polarization techniques, four-photon schemes with Raman resonances (especially CARS) have gained wide acceptance for temperature and concentration measurements in gases [4 – 10, 83 – 86], gas analysis [87], high-resolution molecular spectroscopy [88 – 90], investigations of kinetics and energy-relaxation channels in molecular gases [91, 92], the measurement of dephasing times for molecular vibrations [93, 94] and various multipole components of Raman scattering in atomic vapors [95], studies of photochemical

reactions in laser-excited gas mixtures [96], and other applications. A combination of coherent four-photon probing with selective two-photon population of excited states opens up considerable opportunities for the investigation of population relaxation for excited atomic and ionic states and the measurement of characteristic times of such processes. The potential of such a technique combining two-photon (Raman) excitation (TPE) and CARS probing (TPE – CARS technique [97]) for the measurement of relaxation times of excited states of samarium atoms has been demonstrated in Ref. [98].

Difference-frequency coherent FWM processes in atomic gases, including CARS, have been actively investigated in the context of optical frequency conversion. In particular, Kung [99] reported on the generation of radiation with a wavelength discretely tunable from 117 to 195 nm through FWM in Xe vapor. Optical frequency conversion with the use of resonant FWM was implemented in experiments with Kr [100], Sr [101], Cs [102], and other vapors. A review of studies carried out in this area until the early 1980s was provided by Reintjes [2] and Arkhipkin and Popov [30].

Coherent four-photon Raman spectroscopy of low-temperature laser-produced plasma was implemented in experiments [103], where coherent four-photon scattering involved a Raman transition between excited states of tin atoms. However, FWM schemes with Raman resonances are not always convenient for the diagnostics of highly excited and ionized gas media since the decrease in population differences for excited states of atoms and ions in such media considerably lowers the intensity of the FWM signal [12].

As early as 1973, Régnier and Taran [5] discussed the idea of using wide-beam CARS to image a whole field of parameters of a gas medium. The authors of Refs [104, 105] successfully applied the CARS technique to the investigation of spatial distributions of gas-flow parameters by detecting the multipoint CARS signal produced along a line of intersection of wide pumping beams in a gas flow. The results presented by Jonuscheit et al. [106] suggest that, with a proper arrangement of focusing and collimating optics, CARS can

also provide an efficient means for single-pulse one-dimensional temperature measurements. Significant progress in extracting the data concerning the parameters of a gas medium, which allowed CARS signals from molecules of different sorts to be simultaneously detected, were proposed by the authors of Refs [107–109], who developed a dual broadband CARS scheme, and the authors of Refs [110, 111], who implemented angularly resolved CARS spectroscopy of CO and N_2 molecules.

Among numerous modifications of coherent FWM schemes with Raman resonances, we should mention a technique of three-color FWM involving a dc field [112]. This scheme was proposed as a method for the investigation of dc fields in a gas-discharge plasma by Evsin et al. [113]. The polarization-sensitive modification of this scheme, suggested by Koroteev et al. [114], provides an opportunity to determine the direction and to measure the strength of a dc field in a gas-discharge plasma. The possibility of applying this polarization technique to investigate the statistics of plasma microfields was also discussed in Ref. [114].

2.3 Four-wave mixing with a hyper-Raman resonance
As mentioned above, FWM processes with Raman-type resonances are not always convenient for the diagnostics of the early stages of laser-plasma expansion because of the considerable lowering of the FWM signal intensity due to the decrease in the difference of populations in the levels involved in a Raman resonance, which usually have close energies. Four-wave mixing with hyper-Raman resonances or coherent anti-Stokes hyper-Raman scattering (see the diagram at the right of Fig. 1b) seems to be advantageous in such a situation. The specific features of the amplitude and polarization properties of the hyper-Raman resonant FWM signal stem from the fact that the components of the nonlinear-optical cubic-susceptibility tensor responsible for this process are determined by invariants of the tensor of hyper-Raman scattering (HRS). Hyper-Raman resonances in FWM spectra of a laser-produced plasma were detected for the first time for transitions between excited states of Fe atoms [115]. Subsequently, hyper-Raman FWM spectroscopy was implemented for different atoms and ions produced in a plasma of optical breakdown [24, 116, 117] and in gas-discharge plasmas of the active medium of a copper-vapor laser [14, 22, 24].

The method of coherent four-photon scattering with a one-photon resonance allows experimental determination of important parameters of excited and autoionizing states of atoms and ions in plasmas. In particular, experimental techniques of time-domain and polarization measurements using four-photon scattering with a one-photon resonance have been developed in Refs [25, 118–120]. The method of coherent ellipsometry of autoionizing states on the base of active spectroscopy of hyper-Raman scattering was proposed in Ref. [121]. Hyper-Raman-resonance FWM can be effectively employed as a basis for two-dimensional mapping of relative populations of excited atoms and ions in a low-temperature plasma [35, 122, 123]. This approach is characterized by a high spatial, temporal, and spectral resolutions, thus holding much promise for the investigation of fast processes in spatially nonuniform laser-produced plasmas. However, to extract the information on the parameters of the studied system directly from the experimental spectra of four-photon scattering with a one-photon resonance, one should take into account the phase-matching conditions for waves involved in nonlinear interaction and analyze the influence of the phase mismatch on the shape of the spectrum of four-photon scattering. Resonance one-photon absorption is another important specific feature of this process. Along with dispersion of the medium, resonance one-photon absorption may exert a considerable influence on the shape of the spectrum of radiation emerging from the medium under consideration [124–127].

Similar to FWM with Raman resonances, a combination of hyper-Raman-resonance coherent four-photon probing with a selective two-photon population of excited states opens up new opportunities in measuring the characteristics of excited atomic and ionic states. The advantages of such a combined approach for studying the population of excited states were demonstrated for sodium atoms in a heated cell [128].

Hyper-Raman resonances also offer much promise for enhancing the efficiency of laser-frequency conversion in coherent FWM schemes [129]. This aspect of hyper-Raman-resonance FWM will be considered in greater detail in Section 5.

2.4 Third-harmonic generation
Similar to DFWM, third-harmonic generation (Fig. 1c) is a frequency-degenerate FWM process. However, in contrast to DFWM, phase-matching effects usually play an important role in third-harmonic generation [130]. Third-harmonic generation in gases has been intensively investigated in connection with the conversion of the frequency of high-power laser radiation. Along with excited gas media [2, 131–140], optical-breakdown plasmas have been actively employed for frequency conversion in recent years [36–49]. Although impressive progress has been achieved in high-order harmonic generation and the production of coherent short-wavelength radiation (with a wavelength less than 2.4 nm [141]) in rare-gas jets, an experimental approach employing focused laser beams does not allow efficient frequency conversion even for low-order harmonics. The use of a laser-produced plasma under certain conditions provides an opportunity to achieve comparatively high efficiencies of low-order harmonic generation [36, 37, 45–48].

In the context of nonlinear-optical frequency conversion, much attention has been focused on efficient third-harmonic generation (as well as the generation of higher order harmonics) in hollow waveguides [142]. A considerable (by three orders of magnitude) increase in the efficiency of nonlinear-optical interaction in a hollow dielectric waveguide filled with a gas medium was predicted and experimentally demonstrated for the CARS process by Miles et al. [143] back in 1977, i.e. 20 years before the application of the hollow-fiber technique to THG in short pulses. The idea of using hollow fibers for the compression of ultrashort laser pulses due to another nonlinear-optical process of the third order — self-phase modulation, proposed and implemented by Nisoli et al. [144, 145], proved to be so fruitful that hollow-fiber compressors are currently successfully employed in advanced femtosecond laser systems [146].

Experiments [147] have demonstrated that the phase mismatch due to the gas dispersion in THG in hollow fibers filled with rare gases can be partially compensated due to the dispersion of waveguide modes, which provides an opportunity to achieve a high efficiency of optical frequency conversion in third-harmonic generation (up to 0.2%) and parametric four-wave mixing (up to 13%). Notice that, as

demonstrated in Refs [148, 149], the nonlinear phase shift and the duration of the third-harmonic pulse under these conditions can be controlled due to cross-phase modulation. Experiments in Ref. [147] have stimulated intensive investigations of nonlinear-optical wave-mixing processes in hollow fibers [150, 151]. In particular, it was established that, due to the compensation of phase mismatch in hollow fibers, the efficiency of frequency conversion in high-order (up to the 45th order) harmonic generation can be increased by a factor of 100 – 1000 as compared with the efficiencies of frequency conversion attainable in experiments with gas jets.

Third-harmonic generation can be employed not only for the production of coherent short-wavelength radiation. This effect also provides valuable information on the spectroscopic characteristics of a gas [18] and the dynamics of gas ionization, giving a deeper insight into the specific features of the nonlinear-optical response of an excited atomic system to a strong light field and revealing the channels whereby parameters of excited gas media, including optical discharges, can be controlled.

3. Phase-matching and one-photon absorption effects in coherent FWM

Phase-matching and absorption effects have a considerable influence on coherent FWM with one-photon resonances [126, 127, 152]. The efficiency of the FWM process occurring in a medium with a third-order nonlinearity in accordance with the scheme $\omega_{\mathrm{FWM}} = \omega_1 + \omega_2 - \omega_3$, where ω_1, ω_2, and ω_3 are the frequencies of the pumping waves, is determined by the cubic nonlinear-optical susceptibility of the medium $\chi^{(3)}$ ($\omega_{\mathrm{FWM}}; \omega_1, \omega_2, -\omega_3$) (in what follows, we will omit frequency arguments of the cubic susceptibility for brevity). When the combination of frequencies $\omega_1 + \omega_2 - \omega_3$ is tuned to a resonance with the frequency of a transition between electronic states of an atom or an ion, one can expect a resonant enhancement of the susceptibility $\chi^{(3)}$. However, because of the increase in one-photon absorption at the frequency ω_{FWM} and changes in phase-matching conditions, such enhancement of the cubic susceptibility does not necessarily increase the efficiency of frequency conversion through four-wave mixing.

In this section, we will present the basic relationships allowing a quantitative analysis of the influence of phase-matching and absorption effects on parameters of the FWM signal, qualitatively consider how the regime of FWM changes depending on the relation between characteristic spatial scales of the problem, and analyze the dependence of the FWM signal on the density of resonant species with allowance for phase mismatch and absorption at different stages of the evolution of a laser-produced plasma.

3.1 The basic relationships
To provide a qualitative analysis of the effects of phase mismatch and one-photon absorption, we will employ a formula that describes the power of the FWM signal P_{FWM} at the output of a nonlinear medium for focused pumping beams with Gaussian spatial profiles [2, 153 – 155]:

$$P_{\mathrm{FWM}} \propto \left| \chi_{\mathrm{r}}^{(3)} + \chi_{\mathrm{nr}}^{(3)} \right|^2 P_1 P_2 P_3 G \,. \tag{1}$$

Here, P_1, P_2, and P_3 are the powers of the pumping waves; G is the phase-matching factor; $\chi_{\mathrm{r}}^{(3)}$ is the resonant part of the cubic nonlinear-optical susceptibility of the medium, and $\chi_{\mathrm{nr}}^{(3)}$

is the nonresonant part of the cubic nonlinear-optical susceptibility, which generally includes the quasi-resonant component [25, 26] related to closely spaced resonances of plasma species and transitions involving a continuous spectrum. In the case of focused Gaussian pumping light beams, the phase-matching factor G can be written as [2, 153 – 155]

$$G = 2\pi \int_0^\infty |I|^2 r \, \mathrm{d}r \,, \tag{2}$$

$$I = \exp(-\varkappa_1 L) \int_{-\zeta}^{\xi} \mathrm{d}\xi' \frac{\exp\left[(i\Delta k - \varkappa + \varkappa_1)(\xi - \xi')(b/2) \right]}{(1 + i\xi')(a - i\xi')H}$$
$$\times \exp\left(-\frac{r^2}{H} \right) \,. \tag{3}$$

Here, $\Delta k = k_4 - k'$, $k' = k_1 + k_2 - k_3$; k_4 is the wave vector of FWM radiation in the nonlinear medium; k_1, k_2, and k_3 are the wave vectors of the pump waves in the medium; $\varkappa$ and $\varkappa_1$ are the imaginary parts of the wave vectors k_4 and k'', respectively, $k'' = k_1 + k_2 + k_3$; $a = k''/k'$, $b = 2\pi a_{0i}^2 n(\lambda_i)/\lambda_i$ is the confocal parameter ($i = 1, 2, 3$); a_{0i} is the waist radius of a Gaussian beam with the wavelength λ_i; $\xi = 2(L - f)/b$ and $-\zeta = -2f/b$ are the boundaries of the nonlinear medium written in terms of dimensionless coordinates; f is the coordinate of the center of waists for the pumping Gaussian beams; L is the length of the nonlinear medium, and

$$H = \frac{1 + \xi'^2}{a - i\xi'} + i(\xi - \xi') \,. \tag{4}$$

The resonant part of the nonlinear-optical cubic susceptibility is proportional to the difference of populations N_1 and N_2 in the lower and upper resonance states:

$$\chi_{\mathrm{r}}^{(3)} = (N_1 - N_2)\overline{\chi}_{\mathrm{r}}^{(3)} \,, \tag{5}$$

where $\overline{\chi}_{\mathrm{r}}^{(3)}$ is the resonant cubic nonlinear-optical susceptibility per atom (or ion).

For resonance optical transitions with a Lorentzian spectral line, the expressions for the absorption coefficient and the phase mismatch of linear optical parameters can be written as

$$\varkappa(\delta) = \varkappa_{\mathrm{el}} + \frac{\varkappa_{\max} N_{\mathrm{R}}}{\delta^2 + 1} \,, \tag{6}$$

$$\Delta k(\delta) = \Delta k(0) + \frac{\delta \varkappa_{\max} N_{\mathrm{R}}}{\delta^2 + 1} \,, \tag{7}$$

where $\varkappa_{\max}$ characterizes the resonant contribution of the ionic component to dispersion and absorption of the medium; the terms $\varkappa_{\mathrm{el}}$ and $\Delta k(0)$ describe the nonresonant contribution of the electron component, which can be calculated according to the well-known formulae for plasma dispersion [127, 156]; N_{R} is the concentration of resonant atoms (or ions), and δ is the detuning from the central resonance frequency normalized to the linewidth. In deriving formulae (6) and (7), we assumed that the nonresonant components $\varkappa$ and Δk associated with the contribution of discrete states of atoms and ions are small as compared with resonant components.

As can be seen from formulae (1) – (7), the information concerning the kinetics and spatial distributions of resonant species in temporal and spatial dependences of the FWM

	Four-photon spectrochronography		Coherent ellipsometry		FWM imaging	
	Spectroscopy	Time-domain measurements	Spectral measurements	Time-domain measurements	Point-by-point mapping	Two-dimensional imaging
Measurable parameter	$P_{FWM}(\omega)$	$P_{FWM}(t)$	$\psi(\omega), \chi(\omega)$	$\psi(t), \chi(t)$	$P_{FWM}(\xi_i, \eta_i)$	Image of cross section Σ_i
Information on a medium	$G(\omega)\chi^{(3)}(\omega)$	$G(t)N^2(t)$	$Im\chi^{(3)}(\omega)$ $Re\chi^{(3)}(\omega)$	$P^{(3)}(t)$	$G(x_i,y_i)N^2(x_i,y_i)$	$\{G(x_i,y_i)N^2(x_i,y_i)\}$
Sources of experimental errors and ways to eliminate them						
Problem	Fluctuations of parameters of a medium					
Solution	Broadband scheme	Averaging	Averaging		Averaging	
Problem	Fluctuations of laser parameters					
Solution	Beam referencing					
Solution	Broadband scheme	Averaging	Broadband scheme			
Problem	Phase mismatch and absorption					
Solution	Choosing phase-matched regime with weak absorption / Assessing and correcting for phase mismatch and absorption					
Problem	Interference with coherent background (CB)					
Solution	Polarization CB suppression		Measurements of CB polarization parameters		Polarization CB suppression	
Problem	Interference of spectral lines				Interference of spectral lines	
Solution	Resolving with a polarization technique	Selective study by means of polarization technique	Selective study by means of polarization technique		Selective study by means of polarization technique	

Table 1. Four-photon spectrochronography, coherent ellipsometry, and FWM imaging: P_{FWM} — FWM signal power; G — phase-matching integral; N — density of resonant species; $\chi^{(3)}$ — nonlinear-optical cubic susceptibility of a medium; ψ, χ — tilt angle of the polarization ellipse and ellipticity of the FWM signal; $P^{(3)}$ — third-order nonlinear polarization of a medium; ξ_i and η_i — coordinates in the detector plane (see Table 3 in Section 9); x_i and y_i — coordinates of a point in a medium; curly brackets denote a data array obtained in one measurement.

signal is distorted by the phase mismatch, absorption, and interference of resonant and nonresonant parts of the cubic susceptibility. These effects may also have a considerable influence on the behavior of the FWM signal in the time domain.

In an expanding plasma, the populations N_1 and N_2 of resonant levels and their difference $N = N_1 - N_2$ are functions of time. Therefore, the overall nonlinear-optical susceptibility is also a function of time. Strictly speaking, time-dependent frequency-domain nonlinear-optical susceptibilities (defined as Fourier transforms of time-domain nonlinear-optical susceptibilities) can be consistently introduced only when both $\chi_r^{(3)}$ and $\chi_{nr}^{(3)}$ vary on a time scale much greater than the durations of optical cycles of the light fields involved in the process. In the case of such a hierarchy of time scales, we are dealing with a problem of nonlinear spectro-chronography [31], when the properties of nonlinear-optical susceptibilities have to be determined not only in frequency, but also in the time domains (see Table 1).

The influence of the phase mismatch on the spectrum of one-photon-resonance FWM was investigated in Refs [125 – 127, 156]. In particular, it was demonstrated that, to extract spectral information on the cubic-susceptibility tensor from spectra of four-photon scattering with one-photon resonances, one has to take into consideration the influence of the phase mismatch and one-photon absorption in the medium under study. The influence of one-photon saturation on the spectrum of coherent FWM was considered in Ref. [126]. Saturation effects may be especially important for the analysis of four-photon spectra with one-photon resonances at the frequency of one of the pump waves [24, 116], when high-power pump radiation of the dye laser may noticeably change the populations of electronic states in the atomic or ionic system.

Expressions (1)–(4) can be considerably simplified for several limiting cases. Specifically, compact and physically clear analytical formulae can be derived for the regimes of plane waves [125], tight focusing [126], and strong absorption [127]. However, investigation of phase-matching and absorption effects in the general case usually requires numerical analysis of expressions (1)–(4). The results of numerical simulations with the use of formulae (1)–(7) are discussed in detail in Ref. [127]. Here, we will briefly summarize the main results of the analysis.

First, for high concentrations of resonant atomic species, the dependence of the FWM signal power on the concentration of resonant species may appreciably differ from N^2 (Fig. 2). This circumstance is due to both the increase in the magnitude of one-photon absorption for the FWM wave and the growth of the phase mismatch (parameter Δk increases). Such effects become especially noticeable for large concentrations of resonant atoms. Taking this circumstance into account, we can infer that the increase in the concentration of resonant particles does not necessarily lead to a growth in the efficiency of nonlinear-optical wave mixing. Second, the degree of deviation of the FWM signal power from the quadratic dependence N^2 is determined by the focusing parameters (Fig. 2). Third, the considered dependence of the power of the FWM signal on the concentration of resonant species is sensitive to the frequency detuning δ from one-photon resonance and to the parameter $\varkappa_{max}$. For given parameters of focusing, the character of the studied dependence is determined by the relation between the absorption length and the length of phase matching for the FWM wave.
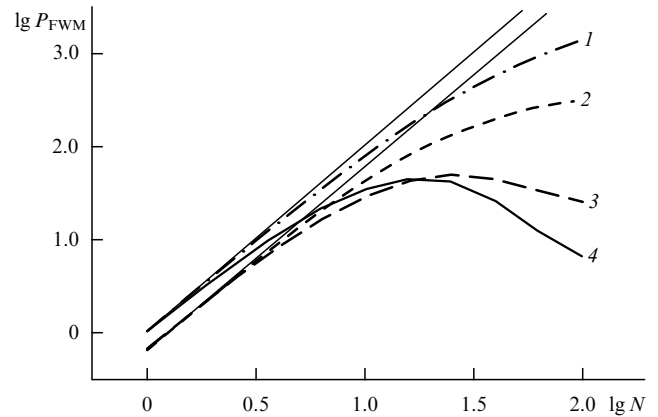
Figure 2. Dependences of the FWM signal power on the concentration of resonant atoms (ions) N with $L = 0.8$ cm, $\varkappa_{max} = 0.1$ cm^{-1}, and $\delta = -1$ for various parameters of focusing: $f = 0.8$ cm (*1, 2*) and $f = 0$ (*3, 4*); $b = 0.8$ cm (*2, 3*) and $b = 0.3$ cm (*1, 4*). The straight lines correspond to quadratic dependences of the FWM signal power.

Fourth, for small detunings from one-photon resonance, the efficiency of nonlinear-optical wave mixing is mainly limited by resonance absorption of the FWM wave. For large detunings, phase matching between the FWM wave and the nonlinear polarization induced in the medium by pumping waves plays an especially important role in coherent FWM, determining the power of the FWM signal.

3.2 Characteristic spatial scales of the problem

Qualitatively, phase-matching and absorption effects in hyper-Raman-resonance FWM can be understood in terms of the following characteristic spatial scales of the problem: the length of phase matching $l_{coh} = \pi/(2|\Delta k|)$; absorption lengths for pumping waves, $l_i = 1/\varkappa_i$ ($i = 1, 2, 3$; $\varkappa_i$ are the nonresonance absorption coefficients at the frequencies of the pump waves), and the FWM signal, $l_{FWM} = 1/\varkappa_r$ ($\varkappa_r$ is the resonance absorption coefficient at the frequency of the FWM signal); the interaction length l_{int} which is determined by the geometry of FWM interaction, and the length l_s that the FWM signal travels from the initial point of the interaction region to the exit of the medium (l_s will be estimated with its upper bound — the length of the medium L). Coherent FWM signal provides information on the concentrations of resonant species free of distortions due to phase mismatch and absorption when the conditions

$$l_{int} < l_{coh}, \tag{8a}$$

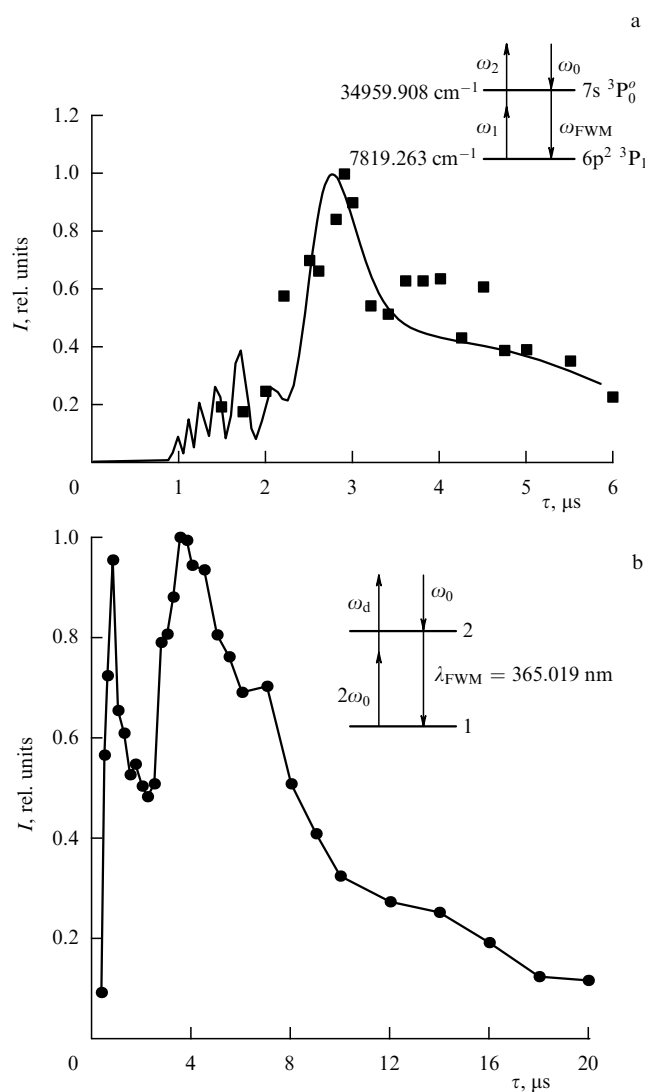$$L < l_{FWM}, l_1, l_2, l_3 \tag{8b}$$

are satisfied.

Generally, the calculation of all the quantities involved in (1)–(7) and, consequently, the characteristic spatial scales introduced above is a rather complex problem. Analysis of this problem in the case of a laser-produced plasma requires certain physical assumptions concerning plasma kinetics. In Refs [24, 117], the optical characteristics of an expanding laser-produced plasma, influencing the efficiency of the FWM process, were calculated with the use of the radiative–collisional model of the kinetics of a multicomponent plasma. Such an approach ensured a satisfactory agreement between the calculated results and experimental data and provides a sufficiently clear understanding of phase-matching and
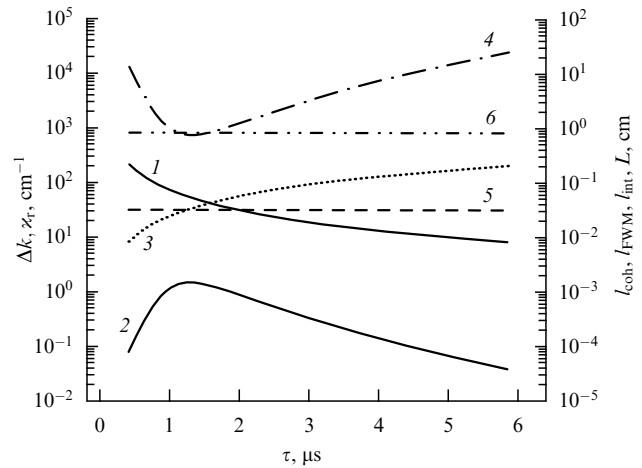
absorption effects in FWM in laser-produced plasmas. Figure 3a presents the experimental time dependence of the FWM signal intensity for a hyper-Raman resonance at the frequency of transition between excited states of lead atoms in a laser-produced plasma. The solid line in Fig. 3a shows the results of calculations performed within the framework of the radiative–collisional model of the kinetics of a multicomponent plasma [160, 161]. Figure 3b displays similar dependences for nitrogen atoms [129].

Figure 4 displays the temporal changes of the phase mismatch Δk, resonance absorption coefficient $\varkappa_r$, and characteristic lengths l_{coh} and l_{FWM} for the FWM process: $\omega_{FWM} = \omega_1 - \omega_0 + \omega_2$ (ω_0 is the frequency of fundamental radiation of a Nd:YAG laser, ω_1 is the frequency of the second harmonic of the Nd:YAG laser, and ω_2 is the dye-laser frequency) with a hyper-Raman resonance at the frequency of transition between the states $7s\,^3P_0^o$ and $6p^2\,^3P_1$ of lead atoms (see the inset to Fig. 3a) in a laser-produced plasma with an initial electron density of 10^{18} cm^{-3} and an initial temperature

Figure 4. Time dependences of the phase mismatch Δk (*1*), resonance absorption coefficient $\varkappa_r$ (*2*), coherence length l_{coh} (*3*), and absorption length of the FWM signal l_{FWM} (*4*) calculated in Ref. [161] for an expanding laser-produced plasma. The interaction length $l_{int} = 0.3$ mm (*5*) for a folded FWM scheme and the length of the medium $L = 1$ cm (*6*) are given for comparison.

of 0.73 eV, expanding in accordance with point-explosion equations [157–159]. The straight lines in Fig. 4 show the interaction length l_{int} for the folded FWM scheme implemented in Refs [160, 161] and the length of the medium L. As can be seen from the dependences presented in Fig. 4, the lengths l_1, l_2, and l_3 remain much greater than the interaction length of a given folded FWM scheme over the entire range of delay times τ between plasma initiation and probing. The absorption length of the FWM signal l_{FWM} under these conditions exceeds the length of the medium L everywhere except for a narrow range adjacent to $\tau = 1.3$ μs, while the coherence length l_{coh} is less than the interaction length for small delay times. With the decrease in the concentration of resonant atoms and electrons in the process of plasma expansion and cooling, the length l_{coh} increases and becomes equal to l_{int} at $\tau \approx 1.2$ μs (the point where curve *3* intersects straight line *5* in Fig. 4). This prediction concerning the behavior of absorption and phase mismatch in a laser-produced plasma is consistent with the results of experiments. Thus, for sufficiently small τ, when $l_{int} > l_{coh}$ and/or $L \sim l_{FWM}$, the dependence of the FWM signal power P_{FWM} on the concentration of resonant atoms may deviate from N^2. In such a situation, a procedure for determining the spatial distributions of excited atoms and ions in a plasma from FWM power maps becomes much more complicated, since it should be performed with allowance made for phase mismatch and one-photon absorption. For $\tau > 2.0$ μs, conditions (8a) and (8b) prove to be satisfied, the power P_{FWM} can be approximated with a quadratic function of N, and the maps of the FWM signal provide undistorted information on the spatial distribution of atoms or ions in a plasma.

4. Experimental technique

In this section, we consider the basic principles and procedures characteristic of the experimental investigation of excited and ionized gases by means of coherent FWM (e.g., see Refs [122, 123]). Figure 5 presents a diagram of the experimental setup for such investigations. This setup consists of a probing laser system, a laser system for the

Figure 3. Intensity of the FWM signal as a function of the delay time between the pulses of three-color pumping and the pulse that is used to produce the spark for a hyper-Raman resonance involving excited states of Pb (a) and N (b) atoms in a laser-produced plasma: solid points — experimental data, solid lines — results of simulations. The insets show four-photon processes in Pb (a) and N (b) atoms.
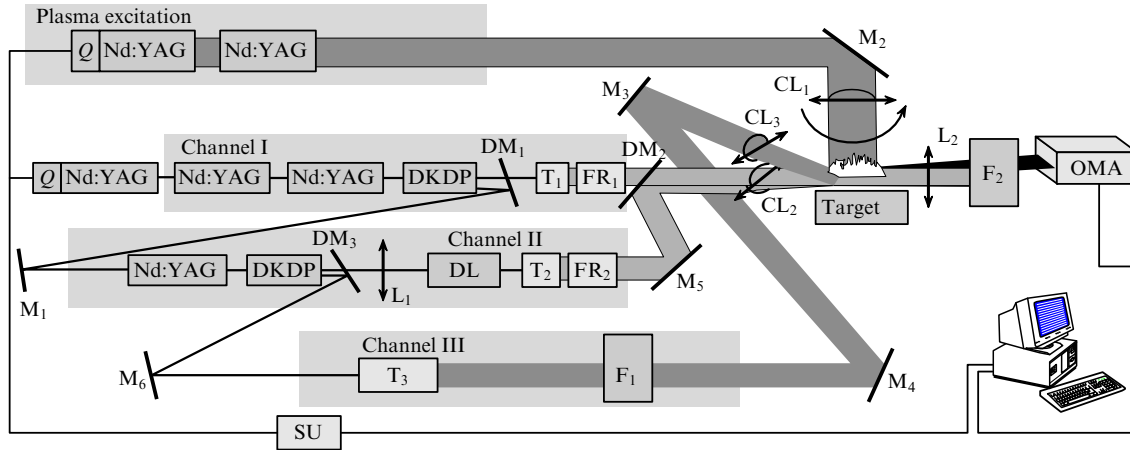
Figure 5. Experimental setup for the investigation of excited and ionized gases by means of coherent FWM in a low-temperature laser-driven plasma [160, 161]: $DM_1 - DM_3$, dichroic mirrors; FR_1 and FR_2, Fresnel rhombi; $M_1 - M_6$, rotating mirrors; $T_1 - T_3$, telescopes; F_1 and F_2, sets of optical filters; OMA, optical multichannel analyzer; SU, synchronization unit; $CL_1 - CL_3$, cylindrical lenses; DL, dye laser, and, finally, L_1 and L_2, spherical lenses.

generation of a plasma of optical breakdown, a synchronization unit, and a detection system.

The probing laser system is built around a Q-switched Nd:YAG master oscillator, which generated laser pulses with a duration $\tau_p = 15$ ns at the wavelength $\lambda_0 = 1.06$ μm (fundamental radiation). The fundamental radiation was amplified with two Nd:YAG amplifiers in channel I and was converted into the second harmonic in a CDA crystal. Radiation that remained unconverted in this crystal was amplified with a Nd:YAG amplifier in channel II and was converted into the second harmonic in a CDA crystal. Second-harmonic radiation was used to pump a dye laser, which generated frequency-tunable radiation within the range $\lambda_d = 0.56 - 0.60$ μm. The polarization of radiation with wavelength $\lambda_0 = 1.06$ μm was fixed, while the polarizations of the second harmonic and dye-laser light beams were varied by means of double Fresnel rhombi in order to ensure the best contrast of FWM spectra. The fundamental radiation with wavelength λ_0, second-harmonic radiation with wavelength $\lambda_0/2 = 0.53$ μm, and the dye-laser radiation with wavelength λ_d were employed as pumping waves in nonlinear-optical interaction in the plasma of optical breakdown. The maximum energies of the pumping waves with wavelengths λ_0, λ_1, and λ_2 were 120, 40, and 5 mJ, respectively. The maximum length of the plasma layer, corresponding to the plasma probing in the longitudinal direction, was 1 cm. In the experiments, we employed both a narrow-band dye laser (with a lasing bandwidth of about 0.5 cm^{-1}) and a broadband dye laser (with a bandwidth of about 200 cm^{-1}). The use of a broadband dye laser made it possible to record FWM spectra of the laser-produced plasma over a rather wide spectral range in a single laser pulse. One of the main problems of broadband FWM spectroscopy is associated with the fact that the use of a broadband dye laser usually gives rise to considerable experimental errors because of spectral fluctuations of the dye-laser radiation [162, 163]. One of the ways to solve this problem is to employ a modeless dye laser [164], which has already proved to be a useful tool for multiplex polarization spectroscopy of plasmas and flames [165 – 167].

The system for plasma initiation was built around a Q-switched Nd:YAG master oscillator. Laser radiation with the

wavelength $\lambda_0 = 1.06$ μm produced by this laser was amplified and focused on the surface of a metal target with a 10-cm-focal-length cylindrical lens. The spark resulting from the breakdown on the surface of the target had a cylindrical shape and was oriented along the direction of propagation of three-color pumping beams. Depending on the energy of the laser radiation and the delay time with respect to spark formation, the plasma studied in our experiments had an electron density $N_e \approx 10^{16} - 10^{19}$ cm^{-3} and an electron temperature $T_e \approx 1 - 10$ eV.

An electric timing unit was designed to synchronize the plasma-excitation and plasma-probing laser pulses. With different delay times, we were able to study linear and nonlinear optical parameters of an ionized gas and to investigate changes in the regime of nonlinear-optical interaction at various stages of plasma expansion.

For the investigation of spectral characteristics of a laser-produced plasma, the FWM signal was analyzed with a polychromator and detected with an optical multichannel analyzer controlled by a personal computer. Such a detection system allowed broadband FWM spectra to be recorded in a single laser pulse, which made it possible to eliminate the influence of inevitable pulse-to-pulse fluctuations of plasma parameters on the accuracy of spectroscopic measurements [122]. For the investigation of spatial distributions of plasma species, the FWM signal generated in the one-dimensional area formed by the intersection of a triad of incident beams was collimated with a cylindrical lens and detected with an optical multichannel analyzer placed behind a set of bandpass filters.

5. Hyper-Raman resonances as a way to enhance the efficiency of FWM in a laser-produced plasma

Recently, much attention has been focused on the problem of generation of coherent short-wavelength radiation by means of optical frequency mixing. In particular, the generation of high-order optical harmonics in rare-gas jets with the use of high-power ultrashort laser pulses provided an opportunity to convert the frequency of laser radiation into the extreme-ultraviolet and soft-X-ray ranges [131–141]. Along with

optical-harmonic generation in rare gases, the possibility of using a low-temperature laser-produced plasma as a nonlinear medium is actively discussed. As has been known for quite a long period of time, laser-produced plasma makes it possible to achieve a sufficiently high efficiency of frequency conversion of Nd:YAG-laser radiation into the third harmonic [36, 37]. Recent experiments [45–48] have demonstrated that the plasma of optical breakdown in gases can be also considered as an efficient source of coherent third-harmonic emission under conditions when high-repetition-rate (1 kHz) femtosecond laser pulses with a moderate intensity (on the order of 10^{15} W cm^{-2}) are used.

The role of excited states of atoms and ions in the generation of optical harmonics and frequency mixing in gases and, in particular, the possibilities of increasing the efficiency of frequency conversion by virtue of intermediate resonances and improving phase-matching conditions in plasmas due to the contribution of bound states, was investigated both theoretically [124, 168] and experimentally [156]. Some of these studies employed the method of four-photon spectroscopy [117]. The feasibility of relying on excited states of atoms and ions for the generation of frequency-tunable radiation in the UV and VUV ranges was clearly demonstrated by a series of experiments (see, for example, Refs [169–171]).

In experiments [116, 117, 122, 123, 160, 161], the use of intermediate hyper-Raman resonances made it possible to considerably increase the efficiency of FWM-signal generation in plasmas, thus allowing a radical improvement in the sensitivity of nonlinear-optical plasma diagnostics based on two- and three-color FWM. In particular, studies [122, 123] were devoted to the investigation of the transition between excited states of nitrogen atoms corresponding to the spectral line centered at 365.019 nm. When the frequency combination $2\omega_0 + \omega_d - \omega_0$ was tuned to a resonance with the transition between the relevant excited states of nitrogen atoms (see the inset to Fig. 3b), an intense resonance in the spectrum of the FWM signal was observed. Notice that, under the above-specified conditions, the signal in the emission spectrum that corresponded to this resonance was relatively weak (the amplitude of this signal was approximately twice as high as the level of background emission). At the same time, the FWM efficiency was so high that the corresponding FWM signal could be observed on a screen placed behind a UFS-2 filter with the naked eye.

The procedure for optimizing the efficiency of nonlinear-optical frequency conversion implied the choice of the optimal delay time between plasma initiation and probing and the optimal geometry of beam focusing for the scheme of three-color pumping. Figure 3b shows the dependence of the FWM intensity on the delay time between the pulses of three-color pumping and the pulse fed to produce the plasma. As can be seen from the experimental data presented, with an appropriate choice of the delay time, the efficiency of nonlinear-optical frequency conversion was considerably increased.

The resonant enhancement of the FWM efficiency was observed within a spectral range with a width of about 0.4 nm. At the maximum of the amplitude–frequency characteristic, the energy of dye-laser radiation was converted into 365-nm radiation with an efficiency of 0.2%. The resonant enhancement in the frequency conversion efficiency at the maximum of the amplitude–frequency characteristic relative to the efficiency of nonresonant FWM measured at 365 nm was

about 10^3 [129]. Within the range of employed radiation energies, the frequency conversion efficiency did not display any noticeable saturation as a function of the intensities of pumping waves, which gives grounds to believe that a further increase in the efficiency of this process can be achieved with the use of picosecond pulses.

6. Four-photon spectrochronography of excited atomic and ionic states

Coherent four-photon spectrochronography is an efficient method for obtaining information on the spectral properties and time evolution of excited atomic and ionic systems [22, 24, 116, 117]. In particular, application of coherent FWM schemes with Raman and hyper-Raman resonances to the investigation of time-dependent spectral parameters of atoms and ions in the plasma of optical breakdown [116, 117] and gas-discharge plasmas [14, 22] provides an opportunity to determine the main features and to measure the characteristics of population relaxation for excited atomic and ionic states.

Early experiments on coherent FWM spectroscopy of atoms, carried out with sodium atoms in flames [58], employed the DFWM technique. This approach provides important spectroscopic information on the properties of excited atomic systems and, as demonstrated by subsequent wide-beam experiments [34], is a convenient way to map the spatial distributions of the parameters of excited atoms in flames. Frequency-nondegenerate coherent FWM schemes, including FWM with Raman and hyper-Raman resonances, permit measurements for atomic and ionic transitions to be carried out over a broad spectral range and open up a wealth of opportunities in polarization control of both line shapes corresponding to isolated resonances and spectral bands related to a group of atomic or ionic transitions with close frequencies (polarization techniques of coherent FWM are discussed in Section 7). Therefore, coherent FWM with Raman and hyper-Raman resonances offers much promise as a scheme of spectrochronographic analysis of excited atoms and ions. Various modifications of coherent four-photon spectroscopy of atoms with Raman and hyper-Raman resonances have been actively employed in recent years for many applied fields, including the investigation of processes determining the efficiency of copper-vapor and copper bromide lasers [14, 22]. CARS spectroscopy of bromine and iodine atoms also provides important information on the distributions of temperature and particles in tungsten–halogen and gas-discharge lamps [172]. In this section, we will consider such experimental techniques in greater detail.
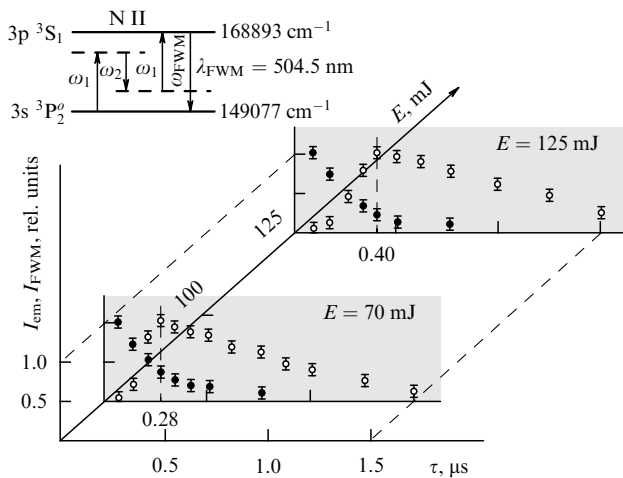
6.1. Laser-produced plasmas
The first experiments on four-photon spectroscopy of atoms in a plasma of optical breakdown on the surface of a solid target were reported in Ref. [103]. The plasma in these experiments was produced by 15-ns radiation pulses of a neodymium garnet laser with an energy of 160 mJ. The second harmonic of a neodymium garnet laser with a frequency ω_1 and dye-laser radiation with a tunable frequency ω_2 were employed as a biharmonic pump. When the frequency difference $\omega_1 - \omega_2$ was tuned to a resonance with the frequency $\Omega = 1736$ cm^{-1} of transition between the $5p^2\,^3P_2$ and $5p^2\,^3P_1$ fine-structure levels of tin atoms, an intense resonance in the CARS spectrum was observed. This

resonance allowed the population kinetics to be investigated for excited states of tin atoms.

This experiment clearly demonstrated that coherent FWM schemes with Raman resonances are efficient for late stages of laser-plasma expansion, permitting the investigation of excited atomic states whose energies are not very high. For the investigation of earlier stages of plasma expansion, it would be important to obtain spectrochronographic information on high-lying atomic and ionic states. This problem can often be solved by means of coherent FWM processes with hyper-Raman resonances [24]. Spectrochronographic and ellipsometric studies of atoms and ions of different charges in a laser-produced plasma with the use of coherent hyper-Raman-resonance FWM have been performed in works [116–120]. The approach based on coherent FWM with hyper-Raman resonances proved to be very efficient for both the investigation of atoms and ions of target elements and the diagnostics of atoms and ions corresponding to ambient-gas elements and the atomic and ionic components of the optical-breakdown plasma produced in cells filled with rare gases [24, 173]. The use of coherent FWM with hyper-Raman resonances furnishes information concerning the population distribution over excited states of atoms and ions in a laser-produced plasma and variations in such population distributions in the process of plasma expansion. Valuable information can be also obtained on the spatial distributions of atoms and ions in plasmas.

Figure 6 presents the time dependences of emission and FWM-signal intensities at the wavelength 504.5 nm corresponding to the transition between the $3s\,^3P_2^o$ and $3p\,^3S_1$ excited states of N II ions (see the top level diagram) [116, 117]. A series of similar FWM resonances was detected within the range of 500.1–500.5 nm, where $3p\,^3D_J \rightarrow 3d\,^3F_{J+1}^o$ transitions ($J = 1, 2, 3$; the wavelengths $\lambda_1 = 500.113$ nm, $\lambda_2 = 500.147$ nm, and $\lambda_3 = 500.514$ nm) of N II ions were observed. For all the spectral lines detected, the intensity of the FWM signal at its spectral maximum was one to two orders of magnitude higher than the emission intensity. It should also be noted that the kinetics of the intensity of hyper-

Raman-resonance FWM signal in a decaying laser-produced plasma considerably differs from the intensity kinetics measured for the same atomic and ionic emission lines (see Fig. 6). In particular, the efficiency of coherent FWM remains sufficiently high to allow reliable diagnostics of the atomic and ionic components of laser-produced plasmas under conditions when the emission of atomic and ionic plasma lines cannot be detected. This difference in time dependences of coherent and incoherent signals is associated with the character of population variations in excited states of atoms and ions in the process of plasma decay.
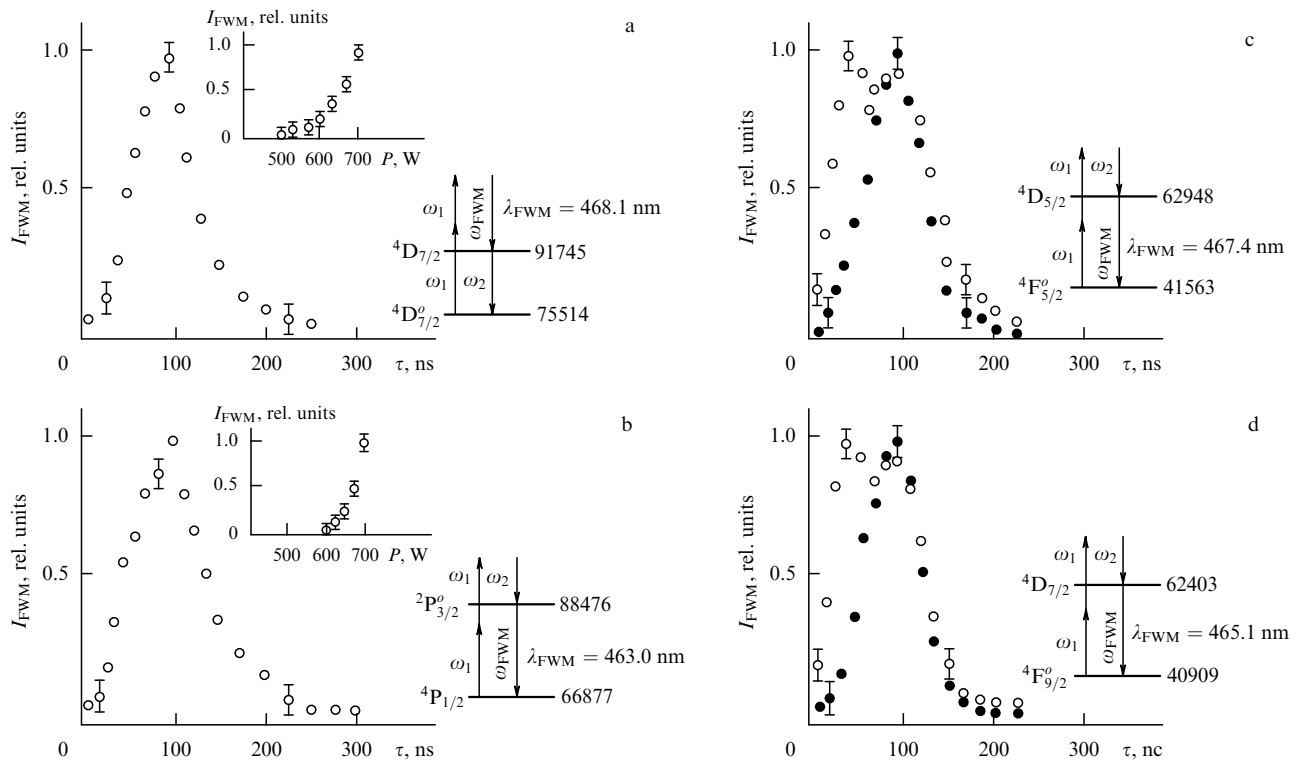
The main specific features of the observed time dependences of the FWM signal and emission intensities in a laser-produced plasma can be qualitatively reproduced within the framework of the quasi-equilibrium radiative–collisional model of an expanding plasma by employing the theory of the modified diffusion approximation (see, for instance, Ref. [174]) with allowance for radiation emitted from the plasma in spectral lines.

6.2. Gas-discharge plasmas

Experiments on coherent four-photon spectroscopy of the atomic component of the gas-discharge plasma employed as the active medium for copper-vapor and copper bromide lasers with small additions of hydrogen were carried out in Refs [14, 22]. These studies have demonstrated that FWM spectra of such plasmas feature resonances related to Raman and hyper-Raman scattering involving excited and autoionizing states of atoms in a gas-discharge plasma. Analysis of the kinetics of the FWM signal under these conditions provides information about population relaxation of excited atomic states.

Experiments were performed with gas-discharge tubes of copper-vapor and copper bromide lasers. The relaxation of the population at the metastable levels in the gas-discharge plasma has a considerable influence on the lasing characteristics of the active media of such lasers [175]. Therefore, the investigation of such processes is important for the improvement of parameters of metal-vapor lasers. Coherent four-photon spectroscopy with hyper-Raman resonances was employed for the investigation of population relaxation from excited metastable states of copper atoms in the active medium of a copper bromide laser with additions of hydrogen. The FWM spectra displayed intense resonances, when the frequency of the FWM signal coincided with the frequency of the $^2P_{3/2}^o \rightarrow {}^2D_{5/2}$ transition (a resonance at the frequency of the FWM signal, $\lambda_{FWM} = 510.5$ nm) and when the dye-laser frequency coincided with the frequency of the $^2P_{1/2}^o \rightarrow {}^2D_{3/2}$ transition (a resonance at the frequency of dye-laser radiation, $\lambda_2 = 578.2$ nm). The characteristic decay times of metastable states of copper atoms in the active medium of a copper bromide laser ($\tau_1 = 1.0 \pm 0.2$ μs for the $^2D_{3/2}$ state, and $\tau_2 = 3.0 \pm 0.4$ μs for the $^2D_{5/2}$ state with the mean power delivered to the discharge plasma equal to 1.3 kW) were measured in Refs [14, 22] and they coincide within the experimental accuracy with the data obtained by other methods [176].

FWM spectra recorded in a gas-discharge tube of a copper bromide laser featured resonances related to transitions between excited electronic states of bromine atoms in the discharge plasma at the wavelength of the FWM signal equal to $\lambda_{FWM} = 468.1$ nm, which corresponds to a resonance of the pump frequency ($\lambda_2 = 616.1$ nm) with the $7d\,^4D_{7/2} \rightarrow 5p\,^4D_{7/2}^o$ electronic transition (the diagram of

Figure 6. Emission intensity I_{em} (•) and intensity of the hyper-Raman resonance FWM signal I_{FWM} (○) as functions of the delay time between plasma excitation and FWM probing for $3s\,^3P_2^o \rightarrow 3p\,^3S_1$ transitions of N II ions in the optical-breakdown plasma. Measurements were performed with energies of plasma-generating radiation $E = 70$ and 125 mJ. The scheme of the CARS process is shown in the top inset.

Figure 7. Kinetics of the intensity of the FWM signal with a hyper-Raman resonance involving excited states of bromine atoms at the wavelengths $\lambda_{FWM} = 468$ nm (a) and $\lambda_{FWM} = 463.0$ nm (b), and copper atoms at the wavelengths $\lambda_{FWM} = 467.4$ nm (c) and $\lambda_{FWM} = 465.1$ nm (d). Open and filled dots represent the FWM signal from the active medium of a copper bromide laser in the absence and in the presence of 0.3 Torr of hydrogen impurity, respectively. Diagrams of four-photon processes employed for the investigation of gas-discharge plasmas are also shown. The insets display the FWM signal intensities as functions of the mean power delivered to the discharge plasma (a, b). The energies of the levels are given in cm^{-1}.

this process is shown in Fig. 7a), and $\lambda_{FWM} = 463.0$ nm, which corresponds to a resonance of the FWM frequency with the $5s\,^4P_{1/2} \to 5p\,^2P_{3/2}^o$ transition (the diagram of this process is shown in Fig. 7b). Figures 7a and 7b present the intensities of FWM radiation as the functions of the delay time and the mean power delivered to the discharge plasma. The diagrams of the employed FWM processes are also shown in these figures. For a fixed delay time equal to 100 ns, the intensity of the FWM signal due to excited Br atoms was measured as a function of the mean power delivered to the discharge plasma (see the insets to Figs 7a and 7b).

As shown in Refs [176, 177], small additions of hydrogen have a considerable influence on the operation of a copper bromide laser. Coherent FWM provides an opportunity to investigate the effect of small hydrogen additions on the kinetics of the population and depopulation of excited atomic states in the active medium of a copper bromide laser. For this purpose, FWM signals produced in the discharge plasma of a copper bromide laser with and without hydrogen additions were detected at the wavelengths $\lambda_{FWM} = 467.4$ nm (Fig. 7c) and $\lambda_{FWM} = 465.1$ nm (Fig. 7d). Measurements were carried out with two identical gas-discharge tubes with a mean power delivered to the discharge equal to 0.7 kW. As can be seen from Figs 7c and 7d, the growth rate of the CARS signal intensity decreases by approximately a factor of two when 0.3 Torr of hydrogen is added to the active medium of the copper bromide laser. Since the efficiency of the FWM process is determined by the square of the population difference for states involved in four-photon scattering, the results of these measurements provide important information about the influence of small hydrogen

additions on the excitation rate and kinetics of relative populations for high-lying levels in a gas-discharge plasma, which can be employed to model the processes in the active medium of a copper bromide laser.

The delivery of high thermal energies at a high pulse repetition rate (up to 20 kHz) to the plasma of active media of metal-vapor lasers leads to the heating of the gas to very high temperatures. Temperature profiles under these conditions may have steep radial gradients over the cross section of the gas-discharge tube [178], which gives rise to spatial inhomogeneities in the spatial distribution of working metal atoms and buffer-gas species [178]. Due to its high temporal and spatial resolutions, coherent four-photon spectroscopy is a useful method for the analysis of the spatial distribution of excited atoms over the cross section and along gas-discharge tubes of metal-vapor lasers. The distribution of the FWM signal intensity over the cross section of a gas-discharge tube of a copper bromide laser with small additions of hydrogen was investigated in the experiments carried out in Ref. [22]. Figure 8 displays the intensities of coherent FWM involving excited copper atoms as functions of the distance from the axis of the gas-discharge tube for the wavelengths $\lambda_{FWM} = 467.4$ nm and $\lambda_{FWM} = 465.1$ nm (Figs 8a and 8b), and similar distributions for excited bromine atoms (Figs 8c and 8d) obtained with a fixed delay time equal to 100 ns.

Four-photon spectroscopy with Raman resonances (two-color CARS) makes it possible to investigate excited states of the $3d^9 4s4p$ configuration of copper atoms in the active medium of a copper-vapor laser. In particular, intense CARS signals detected in experiments at the wavelengths of the anti-Stokes signal $\lambda_a = 510$, 508, and 512 nm [22]
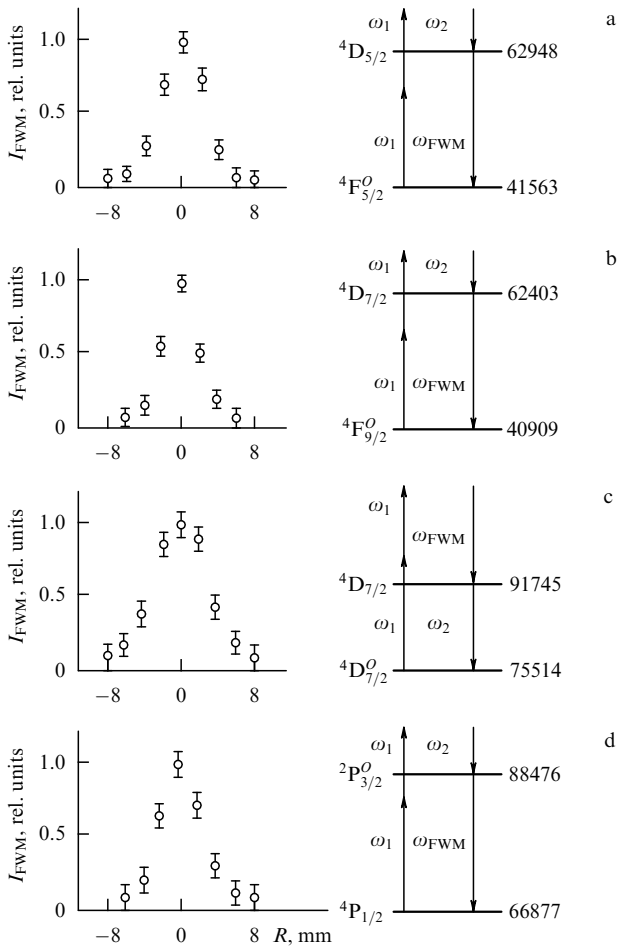
Figure 8. Intensities of FWM signals with hyper-Raman resonances involving $^4F^o_{5/2} \rightarrow {}^4D_{5/2}$ (a) and $^4F^o_{9/2} \rightarrow {}^4D_{7/2}$ (b) transitions between excited states of copper atoms, and $^4D^o_{7/2} \rightarrow {}^4D_{7/2}$ (c) and $^4P_{1/2} \rightarrow {}^2P^o_{3/2}$ (d) transitions between excited states of bromine atoms as functions of the distance R from the axis of the gas-discharge tube for a fixed delay time of 100 ns. The energies of the levels are given in cm^{-1}.

correspond to resonances of the difference frequency $\omega_1 - \omega_2$ with frequencies of $^4P^o_{1/2} \rightarrow {}^4P^o_{3/2}$, $^4D^o_{5/2} \rightarrow {}^4D^o_{7/2}$, and $^4F^o_{3/2} \rightarrow {}^4F^o_{5/2}$ Raman transitions in copper atoms, respectively.

Experiments performed in Refs [14, 22] demonstrated that coherent four-photon spectroscopy with Raman and hyper-Raman resonances is a convenient tool for the diagnostics of gas-discharge plasmas, including the plasma produced in the active media of metal-vapor lasers. The technique of four-photon spectroscopy possesses a high spatial, temporal, and spectral resolutions and allows various schemes of polarization measurements to be implemented. This technique provides useful information on the parameters of plasmas in active media of gas-discharge lasers and, along with conventional methods of linear spectroscopy, can be employed to improve the parameters of gas-discharge lasers.

7. Polarization-sensitive four-photon spectroscopy and coherent ellipsometry of atoms and ions

Methods of polarization-sensitive four-photon spectroscopy provide an efficient tool for the solution of several urgent problems associated with the investigation of atomic and molecular resonances (see Table 1). In particular, properly choosing the polarization vectors of pumping light beams and controlling the polarization state of the signal being detected, one can considerably lower the level of the coherent background due to nonresonant four-wave mixing, which makes it possible to considerably improve the sensitivity of four-photon spectroscopy [3, 122, 123]. Under certain conditions, the polarization technique added to FWM spectroscopy permits one to separately measure the real and imaginary parts of the relevant third-order nonlinear-optical susceptibility [179], to resolve closely spaced lines in FWM spectra of molecules [3, 180] and atoms [26], to increase the contrast of the dispersion curve corresponding to the cubic nonlinear-optical susceptibility near Raman resonances [181, 182], to analyze the interference of vibrational Raman resonances with one- and two-photon electronic resonances in CARS spectra [183], to measure the characteristics of Raman resonances for complex molecules [184], etc. Methods of polarization-sensitive four-photon spectroscopy have been actively developed for more than a quarter of a century (e.g., see Refs [32, 87, 185 – 192]). A comprehensive review of polarization techniques employed for molecular spectroscopy was provided by Akhmanov and Koroteev [3].

The polarization characteristics of radiation emerging from FWM are determined by the properties of the nonlinear polarization of a medium, cubic in an applied field. When analyzing polarization properties of the FWM signal, one should take into account the interference of resonant components of the FWM signal, related to certain (molecular or atomic) transitions in the medium, and the nonresonant coherent background. In particular, it is the interference of the resonant FWM component with the nonresonant coherent background that ensures the possibility of recording complete spectral information concerning the resonance under study, including data on the phase of resonant FWM [53, 118].

Coherent ellipsometry, i.e. the measurement of the parameters of the polarization ellipse corresponding to the FWM signal, is a widely applied modification of polarization-sensitive four-photon spectroscopy. As demonstrated in monograph [3] for Lorentzian lines, coherent ellipsometry makes it possible to separately study the frequency dependences of the real and imaginary parts of the nonlinear-optical cubic susceptibility in many important situations. In Ref. [193], this approach was extended to autoionizing states described by the Fano contour, as well as to the case of a weak resonance with an arbitrary line shape, observed against the background of a strong nonresonant signal. The main principles of coherent ellipsometry of non-Lorentzian spectral lines were developed in Refs [118 – 120].

Plasmas and highly-excited gas media is a new challenging area where polarization methods of coherent FWM can be applied. In this section, we consider in greater detail the polarization technique for resolving closely spaced FWM spectral lines of an arbitrary shape in an optical-breakdown plasma and describe how the information concerning the relative phase of resonant components of FWM signals can be extracted. We will also consider a procedure for reconstructing the frequency and time dependences of the interfering components of the third-order nonlinear polarization of a medium from the data of coherent ellipsometry.

7.1. Polarization properties of the coherent FWM signal from the optical-breakdown plasma

Generally, the parameters of the coherent FWM signal are determined by the properties of the polarization of a medium, cubic in the applied field and induced by pump beams at the frequency of the FWM signal. Along with the intensity of the FWM signal

$$I \propto |P_x|^2 + |P_y|^2, \tag{9}$$

where P_x and P_y are the x- and y-components of the nonlinear polarization of the medium, corresponding to the FWM process under study, we can experimentally examine the ellipticity χ and the tilt angle ψ of the principal axis of the polarization ellipse for the FWM signal. The parameters of the polarization ellipse of the FWM signal can be expressed in terms of the Cartesian components of the total nonlinear polarization of the medium [3]:

$$\tan 2\psi = \tan 2\beta \cos \delta, \tag{10a}$$

$$\sin 2\chi = \sin 2\beta \sin \delta, \tag{10b}$$

where β and δ are given by

$$\tan \beta = \left| \frac{P_y}{P_x} \right|, \tag{11a}$$

$$\delta = \arg P_y - \arg P_x. \tag{11b}$$

As can be seen from formulae (9)–(11), in contrast to the spectrum of the FWM intensity, the frequency dependences of the parameters of the FWM polarization ellipse carry information concerning the phase of the resonant FWM component. Therefore, we have an opportunity to gather information on the real and imaginary parts of the nonlinear resonant polarization of a medium by reference to measured spectral dependences of the parameters of the FWM polarization ellipse.

Analysis of polarization properties of the FWM signal produced in an optical-breakdown plasma shows that the excitation of an atomic system not only increases the efficiency of multiphoton processes due to the population of excited states of atoms and ions [152], but also changes the polarization of the FWM signal [51]. In particular, as demonstrated by experiments [194], the polarization of the FWM signal may remain elliptical even away from resonances. This finding indicates that the third-order nonlinear polarization of a medium away from the resonances under study cannot be represented as a real vector, as is usually done in the analysis of four-photon spectra in the absence of interaction between Raman resonances and electronic states (see Ref. [3]). Notice that the necessity to take into consideration the imaginary part of the nonresonant component of the nonlinear-optical cubic susceptibility in the case of a two-photon resonance or two close Raman-active modes was highlighted back in 1974 in the classical paper by Levenson and Bloembergen [186].

Thus, the FWM signal in excited gases and plasmas is characterized by the presence of an elliptically polarized component of the cubic polarization of a medium, described by a weak function of the frequency. Therefore, in studying the spectra and polarization parameters of FWM in such media, one has to take into account the interference of different components of the nonlinear-optical susceptibility.

Let us consider an FWM process that occurs in accordance with the scheme $\omega_{\text{FWM}} = \omega_1 - \omega_0 + \omega_2$ (in a typical experimental scheme [118–120, 122, 123], ω_{FWM} is the frequency of the FWM signal, ω_0 is the frequency of fundamental radiation of a Nd:YAG laser, ω_1 is the frequency of the second harmonic of the Nd:YAG laser, and ω_2 is the frequency of dye-laser radiation). The vector of nonlinear polarization of the medium $\mathbf{P}^{(3)}(\omega_{\text{FWM}})$ corresponding to the FWM process under consideration can be represented as a sum

$$\frac{\mathbf{P}^{(3)}(\omega_{\text{FWM}})}{E_1 E_2 E_0^*} = \mathbf{P}^{(3)\text{NR}} + \mathbf{P}^{(3)\text{QR}}, \tag{12}$$

where

$$\mathbf{P}^{(3)\text{NR}} = 2\chi_{1111}^{(3)\text{NR}} \left[\mathbf{e}_2(\mathbf{e}_1 \mathbf{e}_0^*) + \mathbf{e}_1(\mathbf{e}_2 \mathbf{e}_0^*) + \mathbf{e}_0^*(\mathbf{e}_2 \mathbf{e}_1) \right] \tag{13}$$

is the vector of nonresonant nonlinear polarization of the medium, $\mathbf{e}_0$, $\mathbf{e}_1$, and $\mathbf{e}_2$ are the unit vectors (which are generally complex) of the polarizations of plane waves at the frequencies ω_0, ω_1, and ω_2, respectively, and $\mathbf{P}^{(3)\text{QR}}$ describes the nonlinear polarization of the medium due to a manifold of quasi-resonant transitions between discrete excited states and continuum of states in a laser-produced plasma. We assume that the nonresonant component $\chi_{1111}^{(3)\text{NR}}$ of the tensor of the cubic susceptibility is described by a real quantity.

Let us examine in greater detail the properties of the vector $\mathbf{P}^{(3)\text{QR}}$, which can be considered as an important characteristic of an excited gas medium. Notice that this quantity does not describe a contribution of any specific atomic or ionic resonance. Rather, it refers to the entire manifold of transitions between excited states whose frequencies are close to the frequencies of incident light waves (or linear combinations of these frequencies). In other words, when we study a specific resonance, this quantity can be considered as a slowly varying function of the frequency as compared with the true resonant component of the third-order nonlinear-optical polarization. Taking into account anomalies in polarization properties of the FWM signal in excited gas media, we can conveniently define the component $\mathbf{P}^{(3)\text{QR}}$ in terms of polarization parameters of radiation. This quantity can be interpreted as a part of the cubic polarization of a medium that is characterized by a weak frequency dependence and that gives rise to an optical signal whose state of polarization generally differs from the polarization state described by relation (13).

Obviously, the information on the quasi-resonant component of the nonlinear-optical susceptibility is important for polarization FWM measurements performed in excited and ionized gases. Therefore, we will consider in greater detail below the available experimental data on this component and describe the experimental procedure of coherent FWM ellipsometry of excited gases and plasmas under conditions when the specific features of polarization of the coherent background should be taken into consideration.

Polarization measurements for two-color four-wave mixing (Fig. 9) demonstrate that, in the absence of a laser-produced plasma, the FWM signal has a linear polarization [194]. Furthermore, the angle θ between the polarization vector of the FWM signal and the polarization vector of radiation at the frequency ω_1 satisfies the relationship $\tan \theta = 1/3 \tan \varphi$, where φ is the angle between the polarization vectors of the pumping waves.
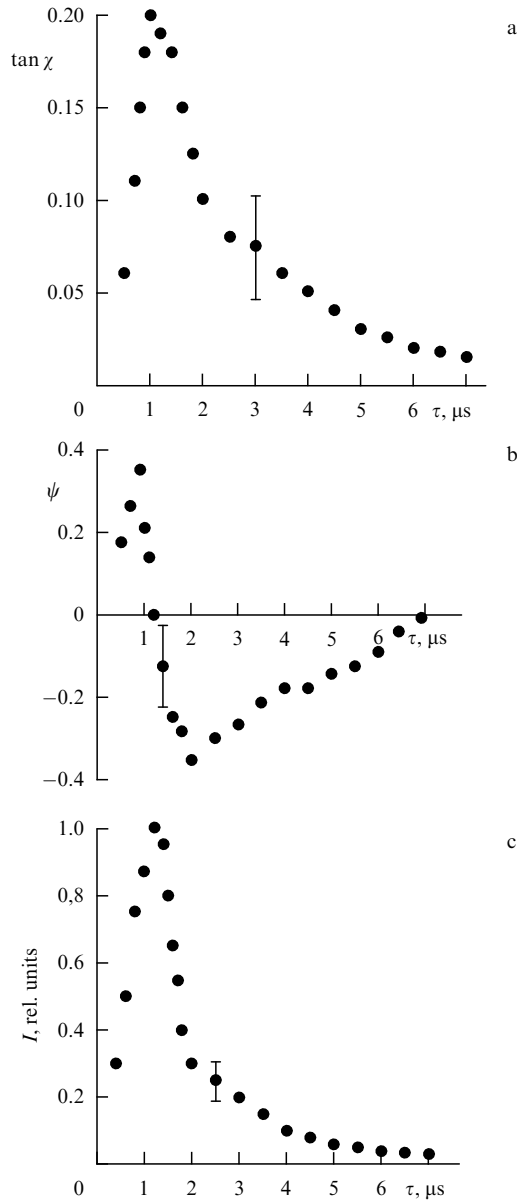
Figure 9. Parameters $\tan\chi$ (a) and ψ (b) of the polarization ellipse and the intensity of the FWM signal (c) as functions of the delay time between the initiation and probing of the laser-produced plasma.

As the system for plasma excitation is switched on, a considerable (by more than an order of magnitude) increase in the intensity of the FWM signal is observed [194]. Simultaneously, radiation at the frequency ω_{FWM} changes its polarization. Measurements performed with the use of phase plates show that the FWM signal from a laser-produced plasma has an elliptical polarization. Figures 9a and 9b display the ratio of the semiaxes of the polarization ellipse, $\tan\chi$, where χ is the ellipticity of the signal, and the tilt angle ψ of the principal axis of the polarization ellipse measured relative to the polarization of the nonresonant FWM signal in the absence of the optical-breakdown plasma. As can be seen from these plots, the parameters of the polarization ellipse considerably depend on the delay time between the excitation and probing of the plasma. Note that the behavior of the studied polarization char-

acteristics correlates with the time evolution of the FWM signal intensity under conditions of optical breakdown (Fig. 9c). For large delay times, the polarization of the signal becomes linear, and the FWM intensity tends to an intensity level characteristic of the nonresonant FWM signal from the air.

The change in the polarization state of the FWM signal under conditions of optical breakdown can be accounted for by the influence of the interference of different components of the nonlinear-susceptibility tensor $\chi^{(3)}$, including the contribution of quasi-resonant bound states of atoms and ions populated under conditions of optical breakdown [25, 26] and the effect of continuum states [121]. Such an interpretation of the above-described experimental results is supported by a qualitative and quantitative correlation between time dependences of the FWM intensity and polarization characteristics of the FWM signal.

The results of experiments [194] demonstrate that the excitation of an atomic system changes the polarization of the FWM signal. The fact that parameters of the polarization ellipse of the FWM signal are sensitive to quasi-resonant components of the nonlinear-optical susceptibility, including the contribution of the states of the continuous spectrum, allows the above-considered experimental technique to be proposed as an efficient scheme of coherent ellipsometry of quasi-resonant atomic systems.

7.2. Separating the real and imaginary parts of the cubic polarization of a medium

As mentioned above, the possibility of reconstructing the data concerning the real and imaginary parts of the nonlinear-optical susceptibility of a medium is due to the interference of the resonant FWM component with the nonresonant coherent background, which ensures the recording of the phase information for the resonance being studied [3, 53, 118]. We begin our analysis of this issue with a class of problems that allow us to assume that the nonlinear polarization of a medium, corresponding to the considered FWM process, can be represented as a sum of the nonresonant and resonant components described by a real vector $\mathbf{P}_{\mathrm{nr}}$ and a complex vector $\mathbf{P}_{\mathrm{r}}$, respectively. Choosing the x-axis along the vector $\mathbf{P}_{\mathrm{nr}}$, we can write the Cartesian components of the total polarization of a medium, cubic in the external field, as

$$P_x = P_{\mathrm{nr}} + P_{\mathrm{r}} \exp(\mathrm{i}\varphi)\cos\alpha, \tag{14a}$$

$$P_y = P_{\mathrm{r}} \exp(\mathrm{i}\varphi)\sin\alpha, \tag{14b}$$

where φ is the phase of the resonant component of the nonlinear polarization, and α is the angle between the resonant and nonresonant components. As follows from the definition of the parameters β and α, these quantities can be found experimentally.

Introducing φ^* to denote the complex phase of P_y, we have

$$\tan\varphi^* = \frac{\sin\varphi}{\cos\varphi + \eta/\cos\alpha}, \tag{15}$$

$$\tan^2\beta = \frac{\sin^2\alpha}{(\cos\varphi\cos\alpha + \eta)^2 + \sin^2\varphi\cos^2\alpha}, \tag{16}$$

where $\eta = P_{\mathrm{nr}}/P_{\mathrm{r}}$ is the ratio of the magnitude of the nonresonant background to the amplitude of the resonant component.

Solving quadratic equation (16) with respect to η, we find

$$\eta = \cos\alpha \left(-\cos\varphi \pm \sqrt{\frac{\tan^2\alpha}{\tan^2\beta} - \sin^2\varphi} \right). \qquad (17)$$

Substituting (17) into (15), we derive the expression for φ^*:

$$\tan\varphi^* = \frac{\pm\sin\varphi^*}{(\tan^2\alpha/\tan^2\beta - \sin^2\varphi)^{1/2}}. \qquad (18)$$

Taking into account that $\delta = \varphi - \varphi^*$, we have

$$\tan(\delta - \varphi) = \frac{\pm\sin\varphi}{(\tan^2\alpha/\tan^2\beta - \sin^2\varphi)^{1/2}}. \qquad (19)$$

Knowing the parameters of the polarization ellipse, we can apply formulae (11a) and (11b) to find δ, whereupon formulae (17) and (19) allow us to determine η and φ. Thus, the above-described procedure of calculation, in principle, makes it possible to find the real and imaginary parts of the resonant nonlinear polarization from the experimental data obtained by means of polarization-sensitive FWM spectroscopy (for $\alpha = 0$, the solution to the considered set of equations becomes ambiguous). Note that, when developing this procedure, we did not employ the information on the line shape of the resonant FWM component in an explicit form. Thus, we can extend the method for determining the spectral dependences of the real and imaginary parts of the third-order nonlinear-optical susceptibility, developed in Ref. [3] for Lorentzian lines, to arbitrary spectral lines, which is especially important for the FWM diagnostics of a laser-produced plasma. Notice also that the opportunities of the above-described procedure are not reduced to the determination of the frequency dependences of the real and imaginary parts of the nonlinear polarization of a medium. An analogous approach can be implemented in the time domain (see Ref. [118]). In other words, applying the proposed technique to the relevant experimental dependences in both the frequency and time domains, we can reconstruct not only the spectra but also the time dependences of the real and imaginary parts of the nonlinear polarization of a medium.

In the important particular case when the resonant component of the FWM signal can be considered as a small correction to the nonresonant component, namely

$$\eta \gg 1, \qquad (20)$$

the general procedure for extracting the information concerning the real and imaginary parts of the nonlinear polarization of a medium can be considerably simplified and allows an illustrative physical interpretation. If condition (20) is satisfied, we derive the following simple relations

$$\psi = \beta\cos\varphi \propto \mathrm{Re}\,P, \qquad (21a)$$
$$\chi = \beta\sin\varphi \propto \mathrm{Im}\,P. \qquad (21b)$$

Thus, the spectral or temporal dependences of the parameters ψ and χ of the FWM polarization ellipse respectively reproduce the spectral or temporal dependences of the real and imaginary parts of the resonant component of the nonlinear polarization of the medium.

In the opposite limiting case of strong resonance, we have the inequality

$$\eta \ll 1, \qquad (22)$$

which is applicable only within the spectral range where the resonant component of the nonlinear polarization of a medium is much greater than the nonresonant component. In this case, we derive the following relations [118, 120]:

$$\psi' = \psi - \alpha = \frac{P_{\mathrm{nr}}\sin(-\alpha)}{P_{\mathrm{r}}}\cos\varphi, \qquad (23a)$$

$$\chi = \frac{P_{\mathrm{nr}}\sin\alpha}{P_{\mathrm{r}}}\sin\varphi, \qquad (23b)$$

where ψ' is the rotation angle of the axis of the polarization ellipse relative to the resonant component. It is convenient to rewrite expressions (23a) and (23b) in a more compact form

$$P_{\mathrm{r}}\exp(\mathrm{i}\varphi) = \frac{P_{\mathrm{nr}}\sin\alpha}{-\psi' + \mathrm{i}\chi}. \qquad (24)$$

Thus, the data of coherent ellipsometry enable one to extract complete information concerning the resonant component of the nonlinear polarization of a medium, including information on the phase of this component (see Table 1).

Expressions presented above were derived with the assumption that the resonant and nonresonant components of the FWM signal can be represented by complex vectors. However, in many situations of practical importance, one of the FWM signal components is elliptically polarized in itself. Specifically, such a situation occurs when a laser-produced plasma is employed as a nonlinear medium. Then, as demonstrated in experiments [194], due to the interference of the contributions of the discrete and continuous spectra, the nonresonant component of the FWM signal may be elliptically polarized. The polarization-sensitive FWM technique was extended to such a situation in Ref. [118].

7.3. Analysis of close and overlapping lines in FWM spectra

Analysis of close and overlapping lines in FWM spectra is an important problem of nonlinear-optical spectroscopy of multicomponent excited and ionized gas media. Monograph [3] provides a comprehensive consideration of the ways this problem can be solved by means of polarization FWM measurements for Lorentzian lines. However, the approximation of Lorentzian contours is not always applicable to the description of atomic and ionic spectral lines in a laser-produced plasma. The expressions derived in Refs [118 – 120] establish the relations between the components of the third-order polarization of a medium and parameters of the polarization ellipse of the FWM signal in the case of non-Lorentzian lines for an arbitrary ratio of the amplitude of the resonant (quasi-resonant) component of the cubic polarization of the medium to its nonresonant part. In Ref. [120], this approach was applied to the analysis of the data of FWM spectroscopy and coherent ellipsometry of low-temperature laser-produced plasmas.

Let us consider the case when the FWM spectrum contains two closely spaced resonances. We will demonstrate that, if the magnitude of one of the resonances is small compared to the other resonance within a certain frequency range (for example, near the maximum of the strong resonance) and we can neglect the influence of the nonresonant background, the weak resonance can be employed as a reference component that stores information concerning the relative phase of the strong resonance.

We assume that the relevant components of the FWM signals are linearly polarized. Suppose that $P_{\mathrm{r}1}$ is the amplitude of polarization of a medium that corresponds to the strong resonance, and $P_{\mathrm{r}2}$ is the amplitude of polarization

of a medium that corresponds to the weak resonance. Assuming that $P_{r1} \gg P_{r2}$, we have [118, 120]

$$\psi' = \psi - \tilde{\alpha} = \frac{P_{r2} \sin(-\alpha)}{P_{r1}} \cos \varphi , \qquad (25a)$$

$$\chi = \frac{P_{r2} \sin \alpha}{P_{r1}} \sin \varphi , \qquad (25b)$$

where the small angle ψ' is measured from the polarization plane of the strong line (which makes an angle $\tilde{\alpha}$ with the x-axis of the laboratory frame of reference), φ is the phase difference for the considered resonant components, and α is the angle between the polarization planes of the resonant FWM components under study. These expressions demonstrate that a weak resonance may play the role of a reference signal that stores information concerning the phase of a closely spaced strong resonance.

Taking the squares of (25a) and (25b) and summing the resulting expressions, we derive

$$|P_{r2}|^2 \sin^2 \alpha = (\psi'^2 + \chi^2)|P_{r1}|^2 . \qquad (26)$$

Formula (26) allows the technique for resolving close lines in FWM spectra, developed in Refs [182, 183], to be extended to spectral lines of an arbitrary shape.

We will illustrate this possibility by considering a pair of close lines in an FWM spectrum from a laser-produced plasma experimentally studied in Ref. [118] with the use of a four-photon process occurring in accordance with a scheme of three-color FWM: $\omega_{FWM} = \omega_1 - \omega_0 + \omega_2$, where ω_{FWM} is the frequency of the FWM signal, ω_0 is the frequency of fundamental radiation of a Nd:YAG laser, ω_1 is the frequency of the second harmonic of a Nd:YAG laser, and ω_2 is the frequency of dye-laser radiation. Intense resonances were observed in the spectrum of four-photon scattering at the frequencies of transitions between excited states of atoms and ions in the optical-breakdown plasma produced on the surfaces of targets of stainless steel. In particular, resonances related to the $^5F \rightarrow {}^5G^o$ transitions between excited states of iron atoms (with a wavelength of 0.3618 μm) and $^3S \rightarrow {}^3P^o$ transitions between excited states of nitrogen N II ions (with a wavelength of 0.3615 μm) were detected in the spectrum of the FWM signal.
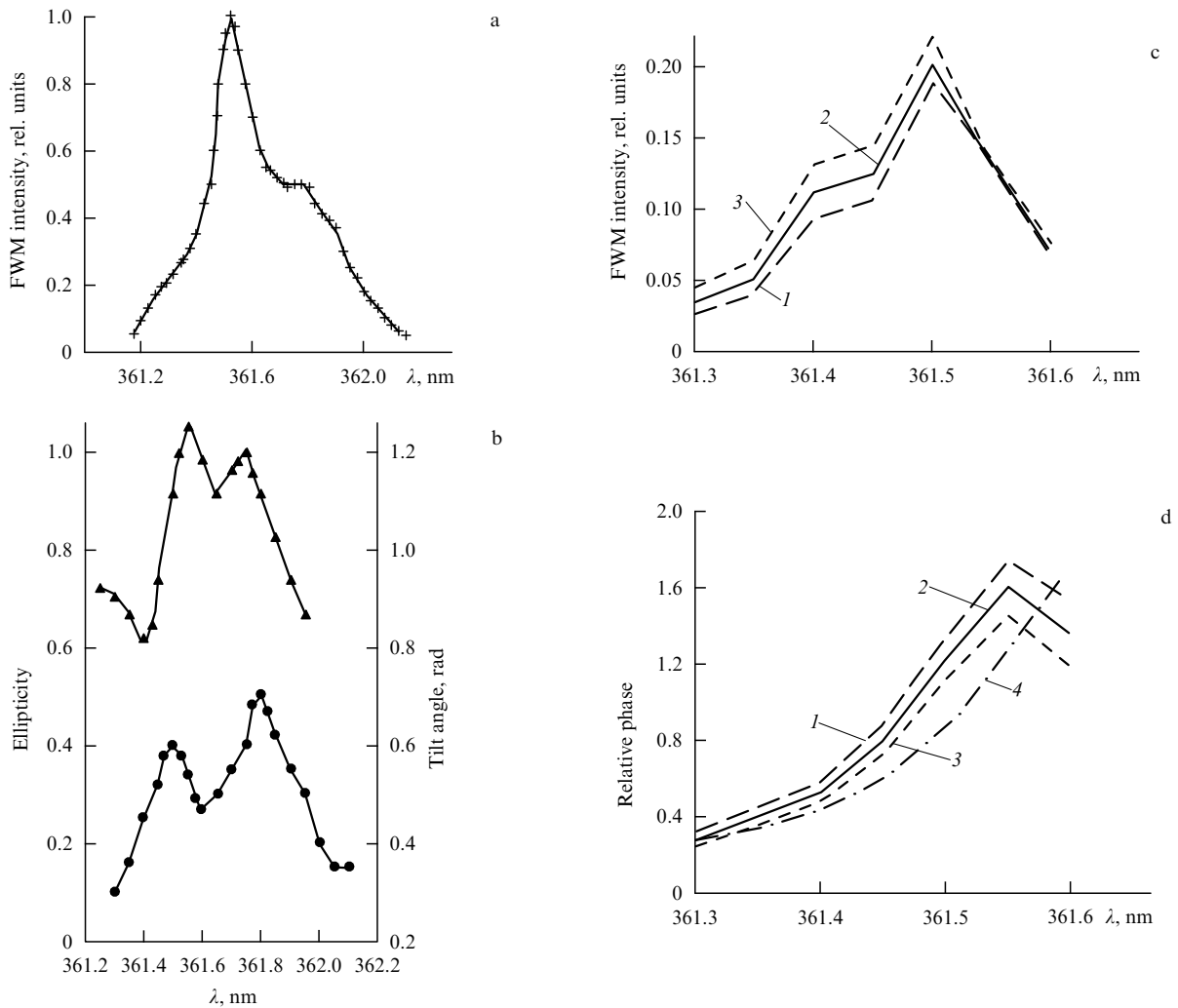
Figure 10. Frequency dependences of the intensity (a), the ellipticity (circles) and the tilt angle (triangles) of the principal axis of the polarization ellipse (b) of the FWM signal near the resonances due to $^5F \rightarrow {}^5G^o$ transitions of iron atoms and $^3S \rightarrow {}^3P^o$ transitions of nitrogen N II ions in the optical-breakdown plasma produced on the surface of a steel target [120]. Data points mark experimental findings for the total FWM signal. The use of the procedure described in the text makes it possible to reconstruct the spectral dependences of the weak resonant component (c) and the phase difference of the resonant components (d). The results of calculations are given for $\tilde{\alpha} = 1.20$ (*1*), $\tilde{\alpha} = 1.25$ (*2*), $\tilde{\alpha} = 1.30$ (*3*), and for Lorentzian resonances (*4*).

As can be seen from Fig. 10a, the intensity spectrum of a three-color FWM signal does not allow us to reliably identify the resonance due to the transitions between excited states of iron atoms. This pair of lines can be analyzed with the use of the following approach [118 – 120]. Let us assume in the first approximation that we can neglect the contribution of the weak component to the intensity of the FWM signal near the maximum of the strong resonance in Fig. 10a, so that the angle ψ' can be set equal to zero and, therefore, $\psi = \tilde{\alpha}$. Next, we apply formula (26) to determine the quantity $P_{r2} \sin \alpha$ within the spectral range from 361.30 to 361.60 nm, assuming that the deviations of the experimentally found parameters ψ and χ of the polarization ellipse (Fig. 10b) from $\tilde{\alpha}$ and 0, respectively, are due to the influence of the weak resonance. In addition, since calculations are performed near the maximum of the strong resonance, we assume that the measured intensity of the FWM signal can be used as an estimate of the quantity $(P_{r1})^2$.

Figures 10c and 10d display the spectral dependences of the weak resonant component and the phase difference of the resonant FWM components, respectively, obtained by means of the above-described procedure. As can be seen from Fig. 10c, for wavelengths greater than 361.50 nm, the conditions of the employed approximation are not satisfied, since the contribution of the left-hand resonance within this region becomes comparable with the contribution of the right-hand resonance. Apparently, the nonmonotone behavior of the spectral dependences of the quantity $P_{r2} \sin \alpha$ and the phase difference within this range is not representative of the real behavior of these parameters. The estimate for the angle $\tilde{\alpha}$ (which corresponded to the angle origin for ψ'), obtained at the initial stage of the procedure, was equal to 1.25 rad (solid curves in Figs 10c and 10d). For comparison, the dashed curves 1 and 3 in Figs 10c and 10d display the dependences that correspond to $\tilde{\alpha} = 1.20$ and 1.30 rad, respectively. The dot-and-dash line in Fig. 10d shows the phase difference for the considered pair of resonances, computed with the assumptions that these resonances, have a Lorentzian shape, the bandwidth of the strong line is 0.1 nm, the bandwidth of the weak line is 0.05 nm, and the separation between the centers of the FWM lines is 0.25 nm [120]. Note that the main difficulty of the procedure for reconstructing the frequency dependence of the weak resonant FWM component and determining the phase difference for the considered pair of FWM resonances is associated with the fact that the ratio of the amplitudes of the considered resonances is about 0.5. Under these conditions, certain precautions should be taken in the application of the proposed approach, especially far from the maximum of the strong resonance. In such a situation, a correct procedure for the reliable reconstruction of frequency dependences for the parameters of a pair of spectral lines, including information on the relative phase of these lines, should employ additional experimental data. It should also be mentioned that the proposed procedure provides information concerning the phase difference of resonant FWM components and does not allow us to separately determine the real and imaginary parts of the relevant closely spaced FWM resonances.

A procedure similar to that described above in this section can be employed to separate interfering components of the third-order polarization of a medium in the time domain. In particular, this technique enables one to reconstruct the time dependence of the relative phase for the relevant components of the FWM signal. Such a procedure was employed in processing the results of coherent FWM ellipsometry of laser-produced plasmas [118]. Importantly, in contrast to amplitude FWM spectra, the frequency dependences of polarization parameters of the FWM signal are insensitive to the phase mismatch and one-photon absorption of light waves involved in FWM [193] (see Table 1), which permits coherent ellipsometry to be applied to the investigation of excited gases and plasmas for obtaining spectroscopic data free of distortions due to phase mismatch and one-photon absorption.

7.4. Polarization control of FWM spectra

A specific feature of broadband FWM spectra is the sensitivity of the relative intensities of spectral lines to the relative polarizations of pumping waves and the orientation of the analyzer. Specifically, varying the angles between polarization unit vectors $\mathbf{e}_0$, $\mathbf{e}_1$, and $\mathbf{e}_2$ and the axis of the analyzer, one can suppress definite components in the FWM spectrum [26] (Fig. 11). Obviously, the possibility of implementing such a polarization control of the shape of a broadband FWM spectrum is very useful for the investigation of multicomponent media, whose spectra usually feature a large number of close and overlapping lines (see Table 1). This experimental technique provides an opportunity to investigate interfering spectral lines corresponding to different components of an excited gas or plasma independently of each other [26, 122, 123] (the fundamentals of the polarization technique in CARS spectroscopy were developed in Refs [182 – 191]).

Physically, the possibility of controlling the shape of FWM spectra stems from the tensor nature of the nonlinear-optical cubic susceptibility of a medium $\chi^{(3)}$ and the fact that the shape of FWM spectra is determined by the interference between the relevant resonant components of $\chi^{(3)}$ and the nonresonant coherent background determined by the nonresonant part of the cubic susceptibility $\chi^{(3)}$. The expression for the intensity I_{FWM} of the FWM signal in this case can be written as [195]

$$\frac{I_{\text{FWM}}}{I_0 I_1 I_2} \propto \left| P^{\text{NR}} \sin \varepsilon + \sum_{\sigma} f_{\sigma}(\Delta_{\sigma}) P^{\text{R}\sigma} \sin(\varepsilon - \theta_{\sigma}) \right|^2 . \quad (27)$$

Here, I_0, I_1, and I_2 are the intensities of the pumping waves, $P^{\text{R}\sigma}$ and P^{NR} are the moduli of the vectors of resonant and nonresonant components of the third-order polarization of the medium, ε is the angle between the axis of the polarization analyzer and the normal to the vector $\mathbf{P}^{\text{NR}}$, $f_{\sigma}(\Delta_{\sigma})$ is the shape of the spectral line, θ_{σ} is the angle between the vectors $\mathbf{P}^{\text{NR}}$ and $\mathbf{P}^{\text{R}\sigma}$, and

$$\mathbf{P}^{\text{R}\sigma} = \overline{\chi}_{1122}^{(3)\text{R}\sigma} \mathbf{e}_2(\mathbf{e}_1 \mathbf{e}_0^*) + \overline{\chi}_{1212}^{(3)\text{R}\sigma} \mathbf{e}_1(\mathbf{e}_2 \mathbf{e}_0^*) + \overline{\chi}_{1221}^{(3)\text{R}\sigma} \mathbf{e}_0^*(\mathbf{e}_2 \mathbf{e}_1) , \quad (28)$$

where $\overline{\chi}_{1122}^{(3)\text{R}\sigma}$, $\overline{\chi}_{1212}^{(3)\text{R}\sigma}$ and $\overline{\chi}_{1221}^{(3)\text{R}\sigma}$ are the components of the resonant cubic susceptibility of the medium.

Resonances in FWM spectra, related to various atomic or ionic transitions (even when they have close frequencies), may have different relations between the relevant components of $\chi^{(3)}$ and may be characterized by different phases with respect to each other and relative to the coherent background. Varying the polarization vectors of the pumping waves and the orientation of the analyzer, we can change the conditions of interference of different components in FWM spectra and, thus, control the shape of the FWM spectrum. This approach can be illustrated by a useful analogy with holography [53],
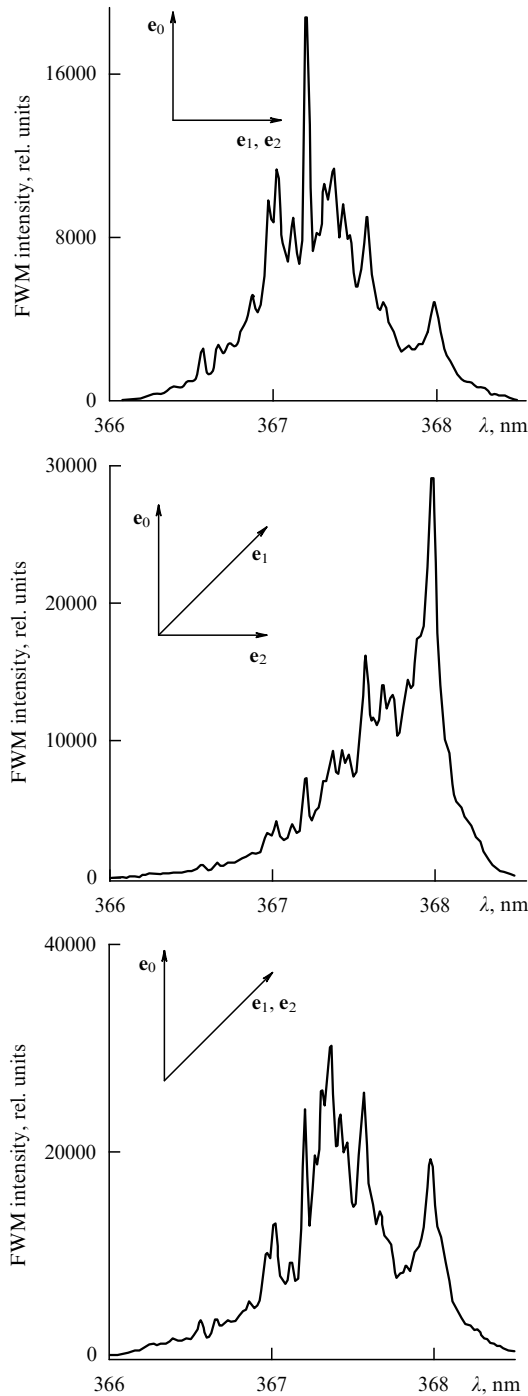
Figure 11. Polarization control of the shape of a broadband FWM spectrum of a multicomponent laser-produced plasma. The relative orientations of the polarization vectors of the pumping waves are shown in the insets.

where the phase information stored in a sample allows one to reveal new details of the recorded pattern by looking at the hologram at various angles. A review of experimental and theoretical studies on what is called holographic multidimensional spectroscopy is provided in Ref. [53].

7.5. Measuring invariants of the tensor of hyper-Raman scattering

The coherent four-photon process with a hyper-Raman resonance in the excited and ionized gas media is related to hyper-Raman scattering (HRS) [3, 22, 24] involving electro-

nic states of atoms and ions. Therefore, the components of the nonlinear cubic susceptibility tensor $\chi^{(3)}$ responsible for this four-wave mixing process can be expressed in terms of irreducible components of the vectorial part of the HRS tensor. Thus, polarization of the FWM signal may provide information concerning HRS tensor invariants.

Let us consider a method of polarization measurements using two-color FWM: $\omega_{\mathrm{FWM}} = 2\omega_1 - \omega_2$ that allows us to determine the relations between HRS tensor invariants [22, 24]. Suppose that the pump waves are linearly polarized, and their polarization vectors make an angle φ with each other. Then, measuring the angle ψ between the polarization vector of the hyper-Raman-resonance FWM signal and the polarization vector of the pump beam at the frequency ω_1, and calculating, in accordance with Ref. [3], the depolarization ratio

$$\rho = \frac{\chi_{1221}^{(3)}}{\chi_{1111}^{(3)}} = \frac{\tan\psi}{\tan\varphi} \, , \tag{29}$$

we can find the ratio of the HRS tensor invariants with the use of the following formula [22, 24]:

$$\frac{\beta_2^{(1)}}{\beta_0^{(1)}} = \sqrt{5}\,\frac{1-\rho}{2\rho+1} \, . \tag{30}$$

Table 2 presents the ratios of irreducible components of the vectorial part of the HRS tensor, calculated with the use of formulae (29) and (30) for excited states of atoms and ions in laser-produced [24] and gas-discharge [14, 22] plasmas by means of polarization-sensitive measurements in two-color FWM with a hyper-Raman resonance.

8. Coherent four-photon spectroscopy of autoionizing states

The investigation of autoionizing (AI) states is of considerable importance for the solution of various fundamental and applied problems [196 – 199]. Specifically, AI states with small bandwidths hold much promise for selective multiphoton ionization of atoms. The cross sections of such transitions involving AI states may be several orders of magnitude higher than the cross sections of direct photoionization through the continuous spectrum, which makes it possible to improve the efficiency of photoionization [200, 201] and generation of UV light [202]. Information on the spectrum of AI transitions is also necessary for various spectroscopic applications, such as the detection of microimpurities and laser isotope separation [203]. At the same time, the study of AI states may provide a deeper understanding of the physics of multielectron atoms. Since AI levels lie above the ionization threshold, the characteristic features of such states are closely connected with the interference of energy levels from discrete and continuous spectra, which results in the modification of the continuous spectrum of an atom. The development of different techniques of nonlinear laser spectroscopy provided an opportunity of studying a broad variety of AI states with different angular momenta [204, 205] that are not necessarily coupled with the ground state of an atom by one-photon transitions. In particular, as demonstrated in Refs [199, 200, 206, 207], valuable information on the properties of autoionizing and autoionizing-like states can be obtained with the use of coherent multiphoton spectroscopy. Elizarov and Cherepkov [208] developed the experi-

Table 2. Ratios of irreducible components of the vectorial part of the HRS tensor, measured by means of the polarization FWM technique for transitions between excited states of atoms and ions in laser-produced and gas-discharge plasmas

Atom/ion	Transition	ρ	$\beta_2^{(1)}/\beta_0^{(1)}$	Method of plasma initiation	References
N II	$3d^3F_2^o \to 3p^3D_1$	-0.31 ± 0.03	7.7 ± 0.9	optical breakdown	[117]
Ar II	$4p^2D_{3/2}^o \to 4s^2P_{1/2}$	4.1 ± 0.4	-0.75 ± 0.09	optical breakdown	[24]
In II	$7g^3G_5 \to 4f^3F_4^o$	-0.10 ± 0.01	3.1 ± 0.5	optical breakdown	[116]
Cu I	$4s^2D_{5/2} \to 4p^2P_{3/2}^o$	-6.9 ± 1.0	-1.4 ± 0.2	gas discharge	[22]
Cu I	$4p^4F_{7/2}^o \to 4s^4D_{7/2}$	0.14 ± 0.03	1.5 ± 0.1	gas discharge	[22]
Cu I	$4p^4F_{5/2}^o \to 4s^4D_{5/2}$	0.08 ± 0.02	1.8 ± 0.1	gas discharge	[22]
Cu I	$4p^4F_{9/2}^o \to 4s^4D_{7/2}$	0.21 ± 0.04	1.2 ± 0.1	gas discharge	[22]
Br I	$5s^4P_{1/2} \to 5p^2P_{3/2}^o$	4.2 ± 0.3	-0.76 ± 0.07	gas discharge	[24]

mental technique based on two-photon polarization-sensitive spectroscopy for identifying the total angular momenta of AI states. Studies [209, 210] were devoted to experimental and theoretical investigation of linear and circular dichroism in the photoionization of Ba atoms through AI states. Finally, the angular distribution of photoelectrons emitted in three-photon ionization of Ba atoms, involving AI states, was studied in Ref. [211].

Resonances in the spectra of four-photon scattering involving AI states were observed for the first time by Armstrong and Wynne [202] in a vapor of metal atoms. Numerous studies have been devoted to the influence of laser-induced autoionizing-like resonances [199] on the efficiency of multiphoton processes in atoms (see, for example, Refs [206, 207]). Autoionizing states of copper atoms in a gas-discharge plasma were investigated in experiments [212], where a CARS process with a resonance between the frequency ω_{FWM} (corresponding to the wavelength $\lambda_{FWM} = 467.4$ nm) and the frequency of transitions between the $^4D_{5/2}$ AI state and the $^4F_{5/2}^o$ discrete excited state of copper atoms was implemented (see the inset to Fig. 12). The AI resonance in the spectrum of hyper-Raman-resonance FWM was studied with both a narrow-band (with a bandwidth $\Delta\omega_2 = 0.5$ cm^{-1}) and a broadband ($\Delta\omega_2 = 16$ cm^{-1}) dye-laser radiation.

The AI resonance in the spectrum of coherent FWM has a characteristic asymmetric shape (the dots in Fig. 12). The shape of the AI resonance in the FWM spectrum can be described with the use of the well-known formula for the nonlinear-optical cubic susceptibility [213]:
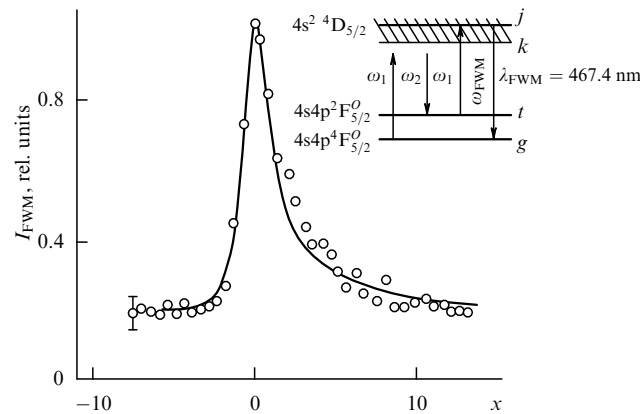
Figure 12. Spectrum of the FWM signal with a hyper-Raman resonance, involving transitions to an autoionizing state of a copper atom: ○ — experimental data, and solid line — results of calculations with formula (35). A diagram of the FWM process is shown in the inset.

$$\chi^{(3)} \propto \sum_{k,t,j} \frac{d_{gj}d_{jt}d_{tk}d_{kg}}{(\omega_{kg}-\omega_1)(\omega_{tg}-\omega_1+\omega_2)(\omega_{jg}-\omega_{FWM})} . (31)$$

Here, d_{gj}, d_{jt}, d_{tk}, and d_{kg} are the matrix elements of the relevant dipole moments, the index g corresponds to the initial state, k and t stand for the virtual states, and j denotes the AI state. In the case under consideration, the difference frequency $\omega_1 - \omega_2$ is close to the frequency ω_{tg} of the $^4F_{5/2}^o \to {}^2F_{5/2}^o$ transition (the detuning is 437 cm^{-1}, Fig. 12). Keeping only one term with the quasi-resonant denominator $\omega_{tg} - \omega_1 + \omega_2 = \Delta\omega$ in the sum in t in expression (31), we derive

$$\chi^{(3)AI} \propto \frac{1}{\Delta\omega} \sum_k \frac{d_{tk}d_{kg}}{\omega_{kg}-\omega_1} \int \frac{d_g(E)d_t(E)}{E-\hbar\omega_{FWM}} \, dE . (32)$$

Thus, similar to Ref. [200], we arrive at the following expression for the nonlinear-optical cubic susceptibility

$$\chi^{(3)AI} \propto \frac{\pi N}{2\omega} d_{g\psi_E}d_{\psi_E t} \frac{q_1q_2 - i(q_1+q_2-x)}{x-i} . (33)$$

Here,

$$N = \sum_k \frac{d_{tk}d_{kg}}{\omega_{kg}-\omega_1}$$

(where integration over the continuum states is implied along with summation over bound states), and

$$x = \frac{E_s - \hbar\omega_{FWM}}{\pi|V_E|^2} ,$$

$$q_1 = \frac{\langle\Phi|d|\varphi_g\rangle}{\pi V_E^*\langle\psi_E|d|\varphi_g\rangle} , (34a)$$

$$q_2 = \frac{\langle\Phi|d|\varphi_t\rangle}{\pi V_E^*\langle\psi_E|d|\varphi_t\rangle} (34b)$$

are the Fano factors, φ_t and φ_g are the wave functions of the bound states (in the case under study, φ_t stands for the wave function of the $^2F_{5/2}^o$ state), ψ_E is the wave function of the state in the continuum, Φ is the wave function of the modified discrete state with the energy E_s, and, finally, V_E is the off-diagonal matrix element [196, 197].

In the regime of tight focusing, which was implemented in experiments [212], the power of the FWM signal can be written as [126]

$$P_{FWM} \propto \frac{(q_1q_2)^2 + (q_1+q_2-x)^2}{x^2+1}$$

$$\times \exp\left[-2\varkappa_0(L-f)\frac{(q_1-x)^2}{x^2+1}\right] (35)$$

(here, we neglected the nonresonant component of the cubic susceptibility).

Fitting the shape of the FWM spectrum calculated with the use of expression (35) to the experimental data, we can determine the Fano parameters q_1 and q_2. Satisfactory agreement between the experimental data and the results of calculations is achieved with $q_1 = -1.8$ and $q_2 = 1.1$ (the solid line in Fig. 12).

Experiments [22, 212] have demonstrated that the investigation of AI states is important for understanding processes that occur in electric-discharge plasmas. The experimental technique developed in Refs [126, 212] makes it possible to determine Fano factors of AI states from experimental spectra of coherent FWM with hyper-Raman resonances. As shown in Ref. [121], valuable information on the interference of the contributions due to the discrete and continuous spectra of an atom can be obtained by means of polarization measurements in FWM spectroscopy. An experimental technique for the investigation of AI states, based on polarization-sensitive resonant FWM, was proposed and substantiated in Ref. [193]. The Fano theory of AI states was used in this paper to derive analytical expressions for the ellipticity and the tilt angle of the principal axis of the polarization ellipse of the light wave resulting from coherent FWM involving AI states. Because of the interference of the contributions due to energy states of discrete and continuous spectra, the FWM signal turns out to be elliptically polarized. Therefore, analysis of the polarization parameters of such an FWM signal allows one to determine the Fano factors for the relevant AI states and provides information on the influence of the atomic continuous spectrum on the nonlinear-optical response of the system. Coherent FWM ellipsometry also makes it possible to separately determine the frequency dependences of the real and imaginary parts of the nonlinear-optical cubic susceptibility near AI resonances.

9. Imaging atomic and ionic plasma components

Physically speaking, the possibility of obtaining information on the spatial distribution of plasma species is based on the fact that the FWM signal intensity is determined by the concentration of particles involved in four-photon scattering (see Table 1). Generally, as can be seen from expressions (1)–(5), the intensity of the FWM signal is a rather complicated function of the concentration of particles because of the interference of resonant and nonresonant components of the cubic susceptibility and because of the influence of phase mismatch and absorption (see Refs [125–127]). However, in those cases when sufficiently intense resonances are observed in the FWM spectrum and the deviation of the concentration dependences of the FWM signal from the quadratic function can be assessed [see formulae (1)–(7)], the coherent FWM signal can be employed to measure the spatial distribution of plasma species (see Tables 1 and 3). In particular, due to the high efficiency of coherent FWM involving some excited atomic and ionic states, this technique is a convenient tool for mapping the spatial distributions of atomic and ionic components in laser-produced plasmas [122, 123] (for the first time this technique was employed to map excited species distributions in a laser-produced plasma in Ref. [215]). Folded wide-beam FWM schemes [5, 34, 104, 105, 214], which can provide single-pulse information on the distributions of atoms or ions in a certain area of a plasma (see Refs

[160, 161] and Tables 1 and 3), are especially promising for this purpose.

In this section, we will discuss how the information on concentrations of resonant species can be extracted from the FWM signal averaged over a series of measurements under conditions when the concentrations of resonant species and the intensities of pumping laser beams are subject to fluctuations. We will consider FWM schemes for point-by-point mapping of atomic spatial distributions in a laser-produced plasma scanned with respect to probing laser beams, and describe FWM methods for the reconstruction of atomic spatial distributions in a laser-produced plasma line by line and slice by slice.

9.1 Coherent FWM with fluctuating parameters of the medium and the pump

Since the coherent FWM signal intensity is a nonlinear (quadratic) function of the density of resonant species, averaging over a series of measurements, which has to be done to smooth out jumps in the FWM intensity from pulse to pulse, gives rise to systematic deviations of FWM images from real spatial distributions of the density of resonant species. In other words, the averaged FWM intensity generally converges to a value other than the square of the mean density of species to be measured [161]. Fluctuations of the intensities of laser beams involved in FWM are another source of experimental errors, when information concerning the spatial distribution of atoms or ions in a plasma has to be extracted from two-dimensional FWM images.

Let us estimate the statistical deviation of the mean power of the FWM signal from the square of the mean density of resonant species for our experiments with optical-breakdown plasmas. Taking into account formula (1), we can express small fluctuations ΔP_{FWM} of the FWM signal power in terms of fluctuation $\Delta(P_1 P_2 P_3)$ of the powers of incident laser beams and fluctuation $\Delta\chi$ of cubic susceptibility $\chi = \chi_r^{(3)} + \chi_{nr}^{(3)}$ (due to fluctuations of plasma parameters):

$$\Delta P_{FWM} = 2a\chi\Delta\chi P_1 P_2 P_3 + a\chi^2 \Delta(P_1 P_2 P_3), \qquad (36)$$

where a is a constant. Then, the relative fluctuation of the FWM power is written as

$$\delta P_{FWM} \equiv \frac{\Delta P_{FWM}}{\langle P_{FWM}\rangle} = 2\delta\chi + \delta(P_1 P_2 P_3), \qquad (37)$$

where $\delta\chi = \Delta\chi/\langle\chi\rangle$ and $\delta(P_1 P_2 P_3) = \Delta(P_1 P_2 P_3)/\langle P_1 P_2 P_3\rangle$, with angular brackets denoting averaging over a series of measurements. Hence, we derive the following expression for the relative variance of the FWM signal power:

$$\frac{\sigma_{FWM}^2}{\langle P_{FWM}\rangle^2} = \frac{\sigma_\chi^2}{\langle\chi\rangle^2} + \frac{\sigma_L^2}{\langle P_1 P_2 P_3\rangle^2}, \qquad (38)$$

where σ_{FWM}^2 is the variance of the FWM signal power, σ_χ^2 is the variance of nonlinear-optical susceptibility, and σ_L^2 is the variance of pump laser powers.

Thus, fluctuations of the FWM signal are determined by fluctuations of the density of resonant species and fluctuations of laser powers. Deviations in FWM images due to fluctuations of the intensities of laser beams can be eliminated with the use of a reference channel, where the coherent FWM signal is produced in some stationary medium simultaneously with the generation of the FWM signal in the main channel
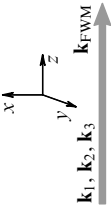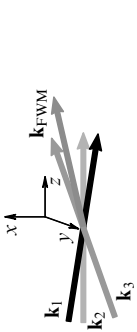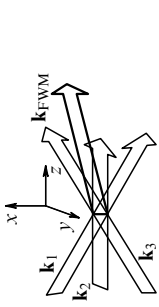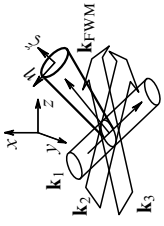
	Collinear FWM in narrow beams	Noncollinear FWM in narrow beams	One-dimensional noncoplanar FWM with wide beams	Two-dimensional noncoplanar FWM with wide beams
Diagram of the process				
How to map spatial distribution	point-by-point scanning	point-by-point scanning	line-by-line scanning	slice-by-slice scanning
How to restore 3D distributions	solving an inverse problem	point by point	line by line	slice by slice
Influence of image-distorting factors — phase mismatch	the entire interaction area	beam intersection area	beam intersection area	beam intersection area
absorption, scattering	the entire interaction area, plus the optical path between the interaction area and the output boundary	beam intersection area, plus the optical path between the interaction area and the output boundary	beam intersection area, plus the optical path between the interaction area and the output boundary	beam intersection area, plus the optical path between the interaction area and the output boundary
Information on instantaneous distributions	maps of averaged parameters	maps of averaged parameters	along lines	in a cross section
Spatial resolution — along $\mathbf{k}_{FWM}$	no resolution	interaction length	interaction length	interaction length
along η	transverse beam size	transverse size of the interaction area	transverse size of the interaction area	resolution of the imaging system
along ξ	transverse beam size	transverse size of the interaction area	resolution of the imaging system	resolution of the imaging system

FWM schemes realized

	Collinear FWM in narrow beams		Noncollinear FWM in narrow beams		One-dimensional noncoplanar FWM with wide beams		Two-dimensional noncoplanar FWM with wide beams
process	CARS	HRRFWM	CARS	DFWM	CARS	HRRFWM	DFWM
object	flames, gas flows, combustion, laser-produced and gas-discharge plasmas	laser-produced and gas-discharge plasmas	flames, gas flows, combustion	flames, gas flows, combustion	flames, gas flows, combustion	laser-produced plasmas	flames, combustion
parameters	$N(x,y)$, $T(x,y)$	$N(x,y)$	$N(x,y)$, $T(x,y)$	$N(x,y)$, $T(x,y)$	$N(x,y)$, $T(x,y)$	$N(x,y)$	$N(x,y)$, $T(x,y)$
References	[3–18]	[115–120]	[110, 111, 228]	[56–66]	[104, 105]	[160, 161]	[34, 70–72]

Table 3. Schemes of coherent FWM for the diagnostics of gas media. $N(x,y)$ and $T(x,y)$ are the spatial distributions of the concentration of particles and the gas temperature, respectively.

(various schemes of beam referencing employed in experiments on coherent FWM are discussed in works [79, 216]). Then, if some fractions of the laser beams involved in coherent FWM are employed to produce the reference FWM signal, this signal is subject to the same deviations due to fluctuations in laser intensities as the FWM signal in the main channel. Therefore, by normalizing the intensity of the FWM signal from a laser-produced plasma to the reference FWM signal, we can get rid of the influence of fluctuations of this type, as the quantity

$$P = \frac{P_{\mathrm{FWM}}}{a P_1 P_2 P_3} = \chi^2$$

becomes measurable in such a scheme, reducing the errors of measurements to those due to fluctuations in the parameters of the medium.

In coherent FWM experiments in laser-produced plasmas [35, 122, 123, 160, 161], fluctuations of the laser power $(\sigma_{\mathrm{L}}^2/\langle P_1 P_2 P_3 \rangle^2 \leqslant 0.01)$ remained much less than the fluctuations of the total FWM signal power $(\sigma_{\mathrm{FWM}}^2/\langle P_{\mathrm{FWM}} \rangle^2 \approx 0.16)$, which allows us to neglect the second term on the right-hand side of Eqn (38). Under these conditions, there is little point in introducing a referencing channel, as it results in a considerable complication of the experimental scheme but does not noticeably improve the accuracy of measurements. In this case, assuming that the laser power does not fluctuate and the quantity χ is characterized by a Gaussian probability distribution, we find that

$$\langle P_{\mathrm{FWM}} \rangle = a P_1 P_2 P_3 \langle \chi^2 \rangle = b \left(\langle \chi \rangle^2 + \sigma_\chi^2 \right), \tag{39}$$

$$\langle P_{\mathrm{FWM}}^2 \rangle = b^2 \langle \chi^4 \rangle = b^2 \left(\langle \chi \rangle^4 + 6\sigma_\chi^2 \langle \chi \rangle^2 + 3\sigma_\chi^4 \right), \tag{40}$$

where $b = a P_1 P_2 P_3$. Using formulae (39) and (40), we derive

$$\langle \chi \rangle = \frac{1}{\sqrt{b}} \left[\frac{1}{2} \left(3 \langle P_{\mathrm{FWM}} \rangle^2 - \langle P_{\mathrm{FWM}}^2 \rangle \right) \right]^{1/4}$$

$$= \frac{1}{\sqrt{b}} \left(\langle P_{\mathrm{FWM}} \rangle^2 - \frac{\sigma_{\mathrm{FWM}}^2}{2} \right)^{1/4}, \tag{41}$$

$$\sigma_\chi^2 = \frac{1}{b} \left(\langle P_{\mathrm{FWM}} \rangle - \sqrt{\langle P_{\mathrm{FWM}} \rangle^2 - \frac{\sigma_{\mathrm{FWM}}^2}{2}} \right). \tag{42}$$

In the case of small fluctuations of the FWM signal, $\sigma_{\mathrm{FWM}}^2/(2\langle P_{\mathrm{FWM}} \rangle^2) \ll 1$, we have

$$\sigma_\chi^2 \approx \frac{\sigma_{\mathrm{FWM}}^2}{4b \langle P_{\mathrm{FWM}} \rangle}. \tag{43}$$

Finally, in the case when the nonresonant part of the cubic susceptibility is small compared with the resonant component, we derive a simple relation between the mean density of resonant particles and measurable statistical characteristics of the FWM signal in the case of small fluctuations of this signal:

$$\langle N \rangle \approx \frac{\sqrt{\langle P_{\mathrm{FWM}} \rangle}}{\chi_{\mathrm{r}}^{(3)} \sqrt{b}} \left(1 - \frac{\sigma_{\mathrm{FWM}}^2}{8 \langle P_{\mathrm{FWM}} \rangle^2} \right). \tag{44}$$

Thus, due to the nonlinear dependence of the FWM signal on the density of resonant species, coherent FWM, in accordance with formulae (39) and (44), generally gives an overestimated value of the density of resonant species.

However, for typical conditions of FWM experiments in laser-produced plasmas [35, 122, 123, 160, 161] with $\sigma_{\mathrm{FWM}}^2/\langle P_{\mathrm{FWM}} \rangle^2 \approx 0.16$, the deviation of the true map of the concentration of resonant particles from the map of the FWM signal was rather small (about 2%).

9.2 Point-by-point two-dimensional mapping of the relative populations of atomic and ionic excited states in a laser-produced plasma

For the experimental investigation of the spatial distribution of the populations in excited states of atoms in an optical-breakdown plasma, a four-photon process $\omega_{\mathrm{FWM}} = \omega_1 + \omega_2 - \omega_0$ can be employed [35, 122, 123, 215], where ω_0 is the frequency of fundamental radiation of a Nd:YAG laser, ω_1 is the frequency of the second harmonic of a Nd:YAG laser, and ω_2 is the frequency of a tunable dye laser. The frequency of the dye laser has to be chosen in such a manner as to ensure a resonance between the frequency ω_{FWM} of the FWM signal and the frequency corresponding to a certain transition between electronic states of atoms excited in a laser-produced plasma (a hyper-Raman resonance).

Generally, studying the intensity of the FWM signal for a spectral component under investigation as a function of spatial coordinates with allowance for phase mismatch and one-photon absorption, one can determine the spatial distributions of the relative populations of resonant atomic or ionic states in a plasma. Representing the measured spatial distribution of the FWM intensity as a two-dimensional gray-scale map, we can visualize the relative populations of the levels involved in a resonance (see Refs [35, 122, 123]). Figure 13 displays two-dimensional maps of the relative intensity of the FWM signal with a resonance at the frequency of the transition between the $7s\,^3P_0^o$ and $6p^2\,^3P_1$ states in Pb atoms and between excited states of N atoms in a laser-produced plasma probed in the longitudinal direction [123]. Similar maps representing the results of transverse plasma probing are shown in Fig. 14. Each point in these maps represents the result of averaging over 100 laser pulses (the correctness of such an averaging procedure was discussed in Section 9.1). The spatial resolution of this point-by-point two-dimensional mapping technique in the plane of plasma scanning (the yz-plane for the longitudinal scheme in Fig. 13, and the xz-plane for the transverse scheme in Fig. 14) was determined by waist sizes of the laser beams employed to generate the FWM signal. For the considered experiments, the maximum waist diameters of the beams were 100 μm. The maps presented in Figs 13 and 14 were obtained in the collinear FWM geometry and are, therefore, not resolved in the direction of probing (along the x-axis for the longitudinal scheme, and along the y-axis for transverse probing).

9.3 The influence of phase mismatch and one-photon absorption

As demonstrated in Section 2, the effects of phase mismatch and one-photon absorption may lead to a deviation of the dependence of the FWM signal power on the concentration of resonant species from a quadratic function, which should be taken into account in experiments on two-dimensional mapping. In this section, we describe the results of measurements that allow direct estimation of the influence of phase mismatch and one-photon absorption on the regime of nonlinear-optical interaction in a laser-produced plasma with the above-specified parameters. Experiments carried out in Refs [122, 123] allowed the intervals of delay times,
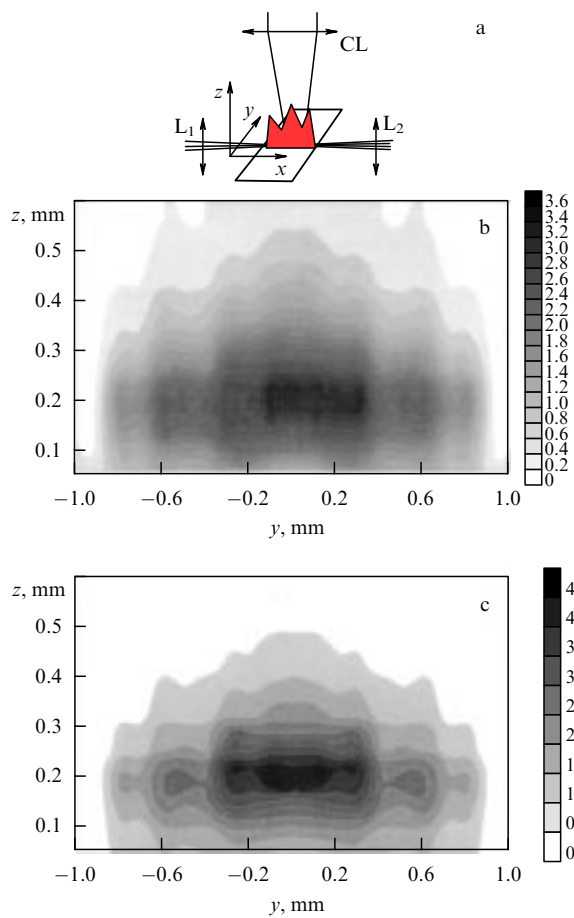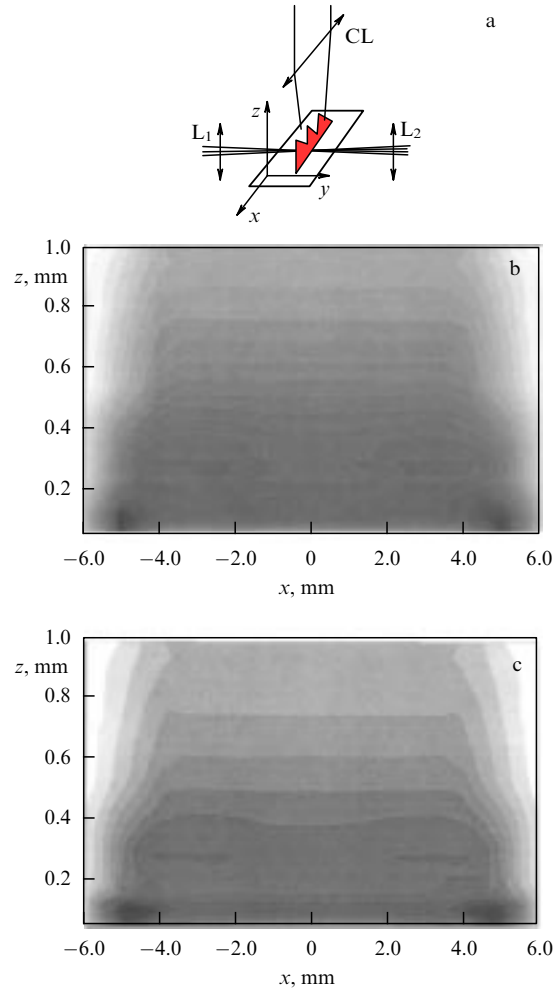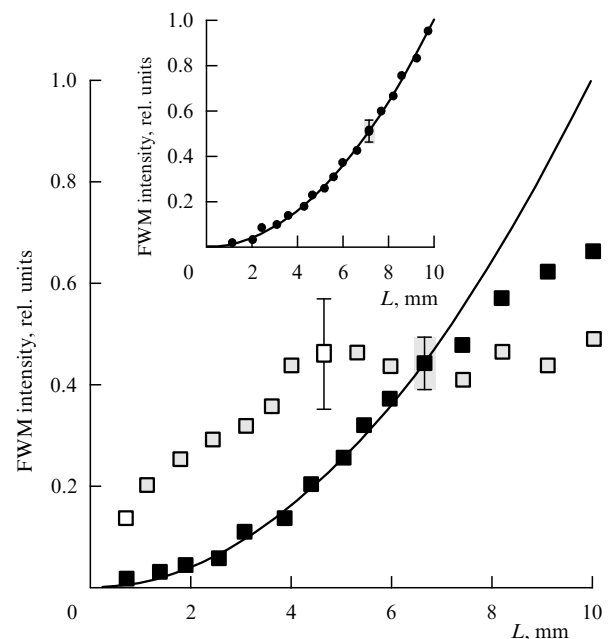
Figure 13. (a) Two-dimensional mapping of the spatial distribution of atoms in a laser-produced plasma probed in the longitudinal direction. (b) Two-dimensional maps of the relative intensity of the FWM signal with a resonance at the frequency of $7s\,^3P_0^o \rightarrow 6p^2\,^3P_1$ transitions in Pb atoms (the wavelength of the spectral line is 368.3 nm), and (c) at the frequency of transitions between excited states of N atoms (the wavelength of the spectral line is 365.0 nm).

Figure 14. Same as Fig. 13 but for transverse probing of a laser-produced plasma.

where resonant and nonresonant FWM interactions occur in the regime close to phase matching and where the influence of one-photon absorption is negligible, to be determined. For this purpose, the power P of the FWM signal at the output of the plasma was investigated as a function of the effective length L of nonlinear-optical interaction in a plasma. The effective interaction length was changed through the variation of the angle between the laser beams involved in FWM and the axis of the laser spark. For this purpose, the cylindrical lens CL_1 (see Fig. 5), which focused laser radiation on the surface of the target, was rotated.

Figure 15 presents the results of such measurements for nonresonant FWM and FWM involving hyper-Raman-type resonances due to the $7s\,^3P_0^o \rightarrow 6p^2\,^3P_1$ transitions in Pb atoms. As can be seen from these plots, the intensity of the nonresonant FWM signal is a quadratic function of the effective interaction length for all delay times τ that might be of practical interest. For small τ, the dependence of P_{FWM} on L in resonant FWM considerably differs from a quadratic function (open squares in Fig. 15). Under these conditions, a procedure of reconstructing the spatial distribution of the relative populations of resonant levels from two-dimensional maps of the FWM signal power is especially complicated, as it should be performed with allowance for phase-matching

Figure 15. Intensity of the FWM signal with a resonance due to $7s\,^3P_0^o \rightarrow 6p^2\,^3P_1$ transitions in lead atoms as a function of the effective plasma length L for $\tau = 0.5$ μs ($\square$) and $\tau \approx 4$ μs ($\blacksquare$). The inset shows the dependence of nonresonant FWM intensity on L.

effects and one-photon absorption. For delay times of the order of 4 µs (full squares in Fig. 15), there exists a range of effective plasma interaction lengths where the dependence of P_{FWM} on L in resonant FWM can be satisfactorily approximated by a quadratic function.

Applying the above-described procedure of measurements, we can estimate, in accordance with formulae (1)–(5), the characteristic length of coherent interaction, i.e. the minimum of l_{coh} and $l_{\mathrm{abs}} = \min(l_i,\ l_{\mathrm{FWM}})$, $i = 1, 2, 3$ parameters. Indeed, since the condition $b > L$ was satisfied for the geometry of measurements in Refs [122, 123], we can lean upon the plane-wave approximation to provide a qualitative description of the experimental results. Therefore, as long as $L < l_{\mathrm{coh}}, l_{\mathrm{abs}}$, one can expect that the intensity of the FWM signal emerging from a laser-produced plasma should scale as the square of the nonlinear-interaction length, as in the case of nonresonant FWM (the inset to Fig. 15) and within a certain range of variation of the effective plasma length in the case of resonant FWM for sufficiently large delay times. For effective interaction lengths greater than 6 mm, the dependence of P_{FWM} on L for large τ noticeably differs from a quadratic function. Hence, for FWM with a resonance at the frequency of the $7s\,{}^3P_0^o \rightarrow 6p^2\,{}^3P_1$ transition in Pb atoms under conditions of the above-described experiments, we have an estimate $\min(l_{\mathrm{coh}}, l_{\mathrm{abs}}) \approx 6$ mm for delay times around 4 µs. For small delay times, the characteristic lengths l_{coh} and l_{abs} are sufficiently small, so that the dependence of the FWM signal power on L substantially differs from the quadratic dependence even for a thin plasma layer. As can be seen from the inset to Fig. 15, nonresonant FWM occurs in the regime when the relations $l_{\mathrm{int}} < l_{\mathrm{coh}}, l_{\mathrm{abs}}$ are satisfied.

Thus, the experimental procedure implemented in Refs [35, 122, 123, 215] makes it possible to quantitatively characterize the influence of one-photon absorption and phase mismatch on the FWM signal power as a function of the concentration of resonant species. The use of the experimental data obtained by means of this procedure in combination with the results of theoretical investigations allows one to perform a correct analysis of the spatial distribution of the populations of excited atomic and ionic states in a laser-produced plasma.

9.4 Two-dimensional mapping of the spatial distribution of atoms in a laser-produced plasma with one-dimensional coherent FWM

As demonstrated in Section 9.2, the main drawbacks of the experimental technique of point-by-point two-dimensional mapping of relative populations of excited atomic and ionic states in plasmas are associated with the fact that such a procedure requires a considerable number of measurements and does not provide resolution in one of the spatial coordinates (see Table 3). Furthermore, since the data concerning the distribution of plasma species for different points of the laser spark are obtained with different sets of laser pulses, i.e. in fact, for different plasma sparks, we need to perform averaging over a certain number of pulses to smooth out jumps in two-dimensional maps resulting from inevitable fluctuations of plasma parameters from pulse to pulse. With such a procedure, we can generate two-dimensional maps only for an averaged spatial distribution of plasma species, which considerably lowers the value of the proposed procedure for the investigation of fast processes in spatially nonuniform media.

These difficulties can be eliminated if one could map a laser-produced plasma in two dimensions using an FWM scheme that would provide information on the spatial distribution of species from a certain area rather than from a single point of the plasma. Multipoint folded FWM schemes, where the FWM signal is generated in the area of intersection of noncollinear pump beams, offer much promise for the solution of this problem. The basic advantage of such an approach is that it provides an opportunity to generate single-pulse two-dimensional plasma images, for instance, to take snapshots of spatial distributions of plasma species, which considerably reduces the losses of useful information. Similar to the techniques recently developed for the investigation of gas flows [217], instantaneous single-pulse plasma imaging would be important, in particular, for the description of plasma media in terms of statistical parameters and for the investigation of spatial correlations of plasma fluctuations. Obviously, the implementation of coherent wide-beam FWM schemes is possible only when the efficiency of the FWM process employed for plasma imaging is high enough to allow a reliable detection of the FWM signal. According to the estimates presented in Ref. [214], such a procedure holds much promise for the investigation of spatially inhomogeneous fast processes in a multicomponent laser-produced plasma.

The experimental technique for two-dimensional imaging of the spatial distribution of atoms in a laser-produced plasma, implemented in Refs [160, 161], was based on a one-dimensional FWM scheme, where the FWM signal was simultaneously generated along a certain line in the plasma (Fig. 16). Similar to the point-by-point mapping technique described above, one-dimensional FWM employed a four-photon process with a hyper-Raman resonance, when the frequency of the FWM signal $\omega_{\mathrm{FWM}} = \omega_1 + \omega_2 - \omega_0$ (where ω_0 is the frequency of fundamental radiation of a Nd:YAG laser, ω_1 is the frequency of the second harmonic of a Nd:YAG laser, and ω_2 is the frequency of a tunable dye laser) was in resonance to the transition between the $7s\,{}^3P_0^o$ and $6p^2\,{}^3P_1$ states of Pb atoms with a wavelength of 368.45 nm (see the inset to Fig. 3a) in a laser-produced plasma. The
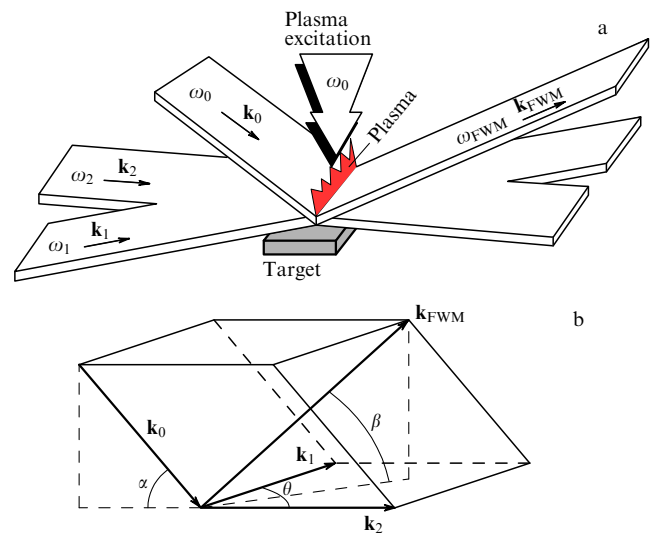
Figure 16. Two-dimensional imaging of spatial distributions of atoms in a laser-produced plasma by means of one-dimensional FWM: (a) a diagram of noncoplanar FWM in wide light beams, and (b) a diagram of the wave vectors.

one-dimensional FWM signal generated in a folded FWM scheme (Fig. 16) was employed to image the spatial distributions of plasma atoms line by line. In this scheme, a pair of cylindrically focused coplanar wide light beams with frequencies $\omega_1 = 2\omega_0$ and ω_2 and wave vectors $\mathbf{k}_1$ and $\mathbf{k}_2$, forming a small angle θ, irradiate a thin plasma layer in a plane parallel to the plane of the target. A cylindrically focused beam with frequency ω_0 and wave vector $\mathbf{k}_0$, which makes an angle α with the plane of the $\mathbf{k}_1$ and $\mathbf{k}_2$ vectors, irradiates the laser-produced spark from above. As this takes place, the FWM signal is generated in the area of intersection of three wide light beams with wave vectors $\mathbf{k}_0$, $\mathbf{k}_1$ and $\mathbf{k}_2$ in the direction $\mathbf{k}_{FWM}$ determined by phase-matching conditions and forming an angle β with the plane of the target. Imaging the one-dimensional FWM signal onto a CCD array allows the spatial distribution of excited lead atoms in a certain cross section of the plasma to be mapped line by line.

The two-dimensional maps shown in Fig. 17 were obtained with $\theta = 0$ and $\alpha \approx 3°$ in the longitudinal (see the top of Fig. 17a) and transverse (see the top of Fig. 17b) schemes of plasma probing. Two-dimensional maps of the spatial distributions of lead atoms were generated line by line through scanning the laser-produced spark with a step of 50 μm along the z-axis. Each of 21 images of one-dimensional FWM, used to generate the two-dimensional maps shown in Fig. 17, represents the result of averaging over 100 laser pulses. The spatial distribution of atoms was mapped under experimental conditions when inequalities (8a) and (8b) were satisfied, i.e. FWM occurred in the coherent regime and absorption effects were negligible. The sensitivity of one-dimensional FWM imaging of lead atoms was estimated as 10^{14} cm^{-3}.

The spatial resolution of three-color folded FWM imaging implemented in Refs [160, 161] is determined by the following factors (see Table 3). The spatial resolution along a CCD array in the direction perpendicular to the wave vector $\mathbf{k}_{FWM}$ (see Fig. 16) is determined by the resolution of the imaging system (objective L_2 in Fig. 5). For the considered one-dimensional scheme of FWM-signal detection, the resolution along the direction perpendicular to the axis of the multichannel analyzer and orthogonal to the wave vector $\mathbf{k}_{FWM}$ is limited by the geometric size of the area where the FWM signal is produced. If a two-dimensional photodetector was used, the spatial resolution in this direction would be entirely determined by the resolution of the imaging system (see the details in Section 9.5).

The one-dimensional FWM scheme employed in Refs [160, 161] does not allow one to resolve coherently emitting sources within the area of intersection of probing beams, determined by the interaction geometry (see Table 3). In particular, the size of this area in experiments [160, 161] was 680×14 μm. Obviously, the spatial resolution of the FWM technique can be improved in this case at the expense of the intensity of the FWM signal, which is proportional to $(l_{int})^2$ in the phase-matched regime in the absence of absorption.

9.5 Prospects of nonlinear-optical methods for the reconstruction of three-dimensional distributions of atoms and ions in laser-produced plasmas
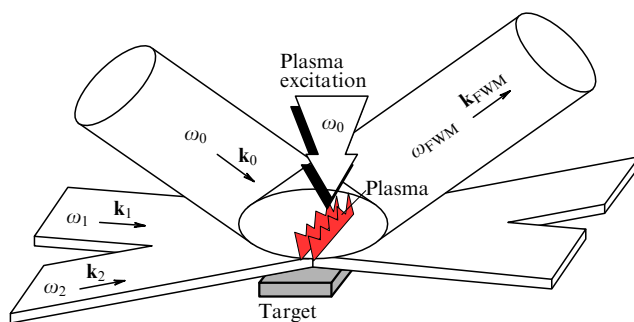
The reconstruction of three-dimensional distributions of physical parameters of an optically thick medium (temperature and concentration of atoms or molecules, flow fields of velocities, turbulence parameters of a flow) from two-dimensional maps of the intensity of light transmitted through such a medium usually requires a rather complicated mathematical procedure [218–220]. Although impressive conceptual and technical progress has been achieved in the development of such methods, especially in connection with
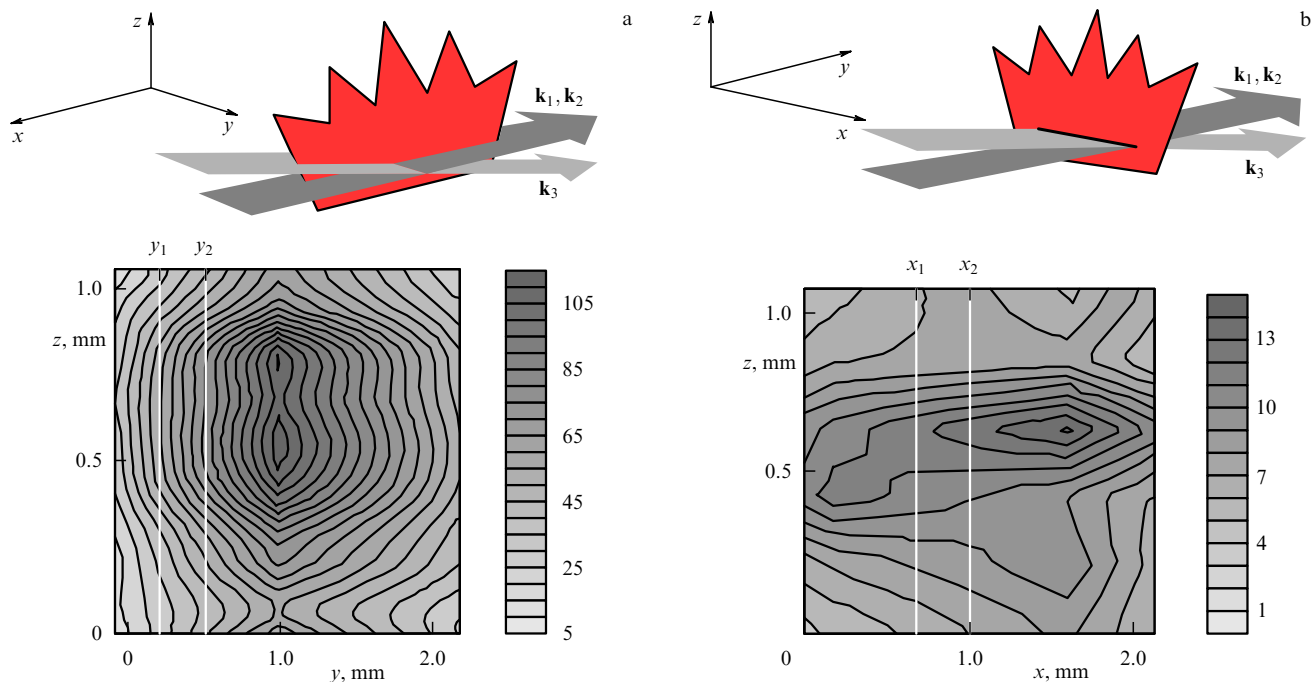
Figure 17. Line-by-line two-dimensional imaging of the spatial distribution of atoms in a laser-produced plasma by means of one-dimensional FWM in the longitudinal (a) and transverse (b) probing directions: top — the schemes of plasma probing, and bottom — two-dimensional maps of the intensity of the FWM signal with a resonance due to $7s\,^3P_0^o \rightarrow 6p^2\,^3P_1$ transitions in Pb atoms (with a wavelength of 368.45 nm). The vertical white lines in Fig. 17a show the slice $y_1 - y_2$ mapped in Fig. 17b, while the vertical white lines in Fig. 17b show the slice $x_1 - x_2$ mapped in Fig. 17a.

medical applications [221] and plasma tomography [222–225], alternative techniques capable of providing information about the spatial distribution of physical parameters in optically thick media are still in great demand. In contrast to tomographic reconstruction of three-dimensional spatial distributions of physical parameters, which requires a series of measurements with subsequent solution of the relevant inverse problem, coherent folded broad-beam FWM allows such spatial distributions to be reconstructed from direct measurements (see Table 3).

In Section 9.4, we discussed an experimental technique that provides an opportunity to reconstruct distributions of excited atoms in a certain cross-section of a plasma line by line. Although such an approach requires fewer measurements than a point-by-point technique, a considerable number of measurements should still be performed to compose the resulting two-dimensional image. A straightforward generalization of the above-described multipoint FWM technique for plasma diagnostics is to extend the plasma imaging to two dimensions. With such an approach, the information on the spatial distribution of species in laser-produced plasmas can be extracted slice by slice rather than line by line. Ewart et al. [34] have employed wide-beam DFWM to image spatial distributions of atoms in a flame. A frequency-nondegenerate FWM technique for the reconstruction of three-dimensional distributions of atoms in a laser-produced plasma slice by slice has been proposed and substantiated by Akimov et al. [214]. In this scheme (Fig. 18), a sheetlike beam irradiating a plasma from above is replaced by a collimated beam that has the shape of a cylinder whose axis makes an angle α with the plane of the $\mathbf{k}_1$ and $\mathbf{k}_2$ vectors, which is parallel, as before, to the plane of the target. The FWM signal is generated in a two-dimensional area of intersection of pumping laser beams in the direction determined by phase matching, carrying information concerning the distribution of physical parameters of a plasma in this area. Imaging the interaction region onto a CCD matrix in FWM light, one can reconstruct the three-dimensional distribution of plasma parameters slice by slice.

Figure 18. Slice-by-slice reconstruction of the three-dimensional distribution of the atomic density in a laser-produced plasma with the use of two-dimensional folded wide-beam FWM [214].

The spatial resolution of this method of imaging along ξ- and η-directions perpendicular to the wave vector $\mathbf{k}_{FWM}$ (see Fig. 18 and Table 3) is determined by the resolution of the imaging system (objective L_2 in Fig. 5). As demonstrated in Ref. [226], if the intensity of the FWM signal is sufficiently high and an appropriate objective is used, the resolution in

these directions may be sufficient for the implementation of coherent FWM microscopy schemes, similar to the scheme described in Ref. [227]. Spatial resolution along the vector $\mathbf{k}_{FWM}$ is determined in this case by the length of the beam interaction area and depends on the interaction geometry.

An obvious advantage of the approach described above over line-by-line imaging is that such a technique would provide an opportunity to generate two-dimensional images of plasma parameters with a single laser pulse, i.e. to take snapshots of whole plasma sections. Such an approach would be especially useful for the investigation of spatially inhomogeneous fast processes in a laser-produced plasma.

Table 3 summarizes the potential of different methods for the reconstruction of spatial distributions of plasma parameters, based on coherent FWM. As can be seen from this table, going over from the collinear FWM scheme to a folded one [228], we improve the locality of the information on the properties of a medium. In contrast to the collinear scheme, the noncollinear technique does not require the solution of an inverse problem for the reconstruction of spatial distributions of physical parameters from FWM intensity measurements integral in the interaction length with allowance for phase mismatch and absorption. However, if the parameters of the medium under study fluctuate from pulse to pulse (as in the case of a laser-produced plasma), the point-by-point scheme allows only the mean values of parameters to be mapped. In this case, wide-beam folded FWM schemes implying the imaging of a two-dimensional FWM signal carrying information on the instantaneous distribution of physical parameters in some cross section of a medium, may provide much more useful data. Importantly, collinear schemes of point-by-point FWM measurements generally provide no resolution along the direction of the vector $\mathbf{k}_{FWM}$, while the resolution along transverse ξ- and η-directions is limited by the sizes of focused pump beams. As we pass from the noncollinear scheme of point-by-point measurements to two-dimensional FWM imaging through the intermediate scheme of one-dimensional FWM, the spatial resolution becomes less and less sensitive to the interaction geometry and is more and more dependent on the resolution of the imaging system (shaded cells of Table 3), which eventually allows FWM microscopy schemes, similar to that demonstrated in Ref. [227], to be implemented.

10. Conclusions

The results of recent experimental and theoretical studies on coherent FWM, discussed in this review, demonstrate that the variety of coherent FWM methods for the investigation of excited and ionized gases currently involves a unique combination of experimental schemes providing frequency- and time-domain (spectrochronographic) information on excited gas media (above all including atomic and ionic components of such media), allowing separate components of complex nonstationary gas and plasma systems to be selectively investigated with the use of the polarization-sensitive FWM technique and coherent ellipsometry, and also permitting nonlinear-optical imaging of spatial distributions of atoms and ions in excited gases and plasmas.

We have considered novel applications of two-dimensional imaging based on coherent FWM with hyper-Raman resonances. Experiments carried out in this direction demonstrate that such an approach can be efficiently used for the investigation of spatial distributions of physical parameters in

excited and ionized gas media, including optical-breakdown and gas-discharge plasmas. In particular, wide-beam coherent FWM provides an opportunity to implement two-dimensional mapping of the relative populations of excited states of atoms and ions in a low-temperature laser-driven plasma produced at the surface of a metallic target. This experimental approach is characterized by a high spatial, temporal, and spectral resolutions and is, therefore, especially useful for the investigation of fast spatially nonuniform processes in a laser-produced plasma. The polarization dependence of FWM spectra allows the sensitivity and selectivity of coherent spectrochronography of multicomponent excited gas media to be considerably enhanced and the contrast of FWM images of such media to be appreciably improved.

Intermediate resonances at the frequencies of transitions between excited states of atoms make it possible to considerably (by several orders of magnitude) increase the efficiency of nonlinear-optical frequency conversion in a laser-produced plasma, thus radically improving the sensitivity of coherent FWM plasma diagnostics. Polarization-sensitive broadband FWM spectroscopy permits one to record spectra of multicomponent optical-breakdown plasmas with a single laser pulse, which provides an opportunity to eliminate the influence of inevitable pulse-to-pulse fluctuations of plasma parameters on the accuracy of spectroscopic measurements and allows one to extract information concerning joint spatial distributions of different plasma components, using a single pulse of a laser spectrometer. Application of the polarization technique to FWM spectroscopy of plasma enables active control of the shape of the FWM spectrum, which makes it possible to suppress or enhance certain components in the FWM spectra. Due to these properties, the proposed experimental technique provides an opportunity to investigate the spatial distributions of the intensities of interfering spectral lines independently of each other.

Coherent FWM ellipsometry allows one to resolve closely spaced atomic and ionic lines in FWM spectra and, in some cases, to perform an independent spectrochronographic analysis of the real and imaginary parts of the nonlinear-optical cubic susceptibility of a medium. Under certain conditions, coherent FWM ellipsometry makes it possible to reconstruct spectral dependences of interfering lines in FWM spectra and to extract the data concerning the phase difference for resonant components of the third-order nonlinear polarization of a medium.

References

1. Shen Y R *The Principles of Nonlinear Optics* (New York: John Wiley & Sons, 1984) [Translated into Russian (Moscow: Nauka, 1989)]
2. Reintjes J F *Nonlinear Optical Parametric Processes in Liquids and Gases* (New York: Academic Press, 1984) [Translated into Russian (Moscow: Mir, 1987)]
3. Akhmanov S A, Koroteev N I *Metody Nelineĭnoĭ Optiki v Spektroskopii Rasseyaniya Sveta* (Methods of Nonlinear Optics in Light Scattering Spectroscopy) (Moscow: Nauka, 1981)
4. Eckbreth A C *Laser Diagnostics for Combustion Temperature and Species* (Energy and Engineering Science Series, Vol. 7) (Tunbridge Wells, Kent: Abacus Press, 1988)
5. Régnier P R, Taran J P-E *Appl. Phys. Lett.* **23** 240 (1973)
6. Harvey A B, Nibler J W *Appl. Spectrosc. Rev.* **14** 101 (1978)
7. Eckbreth A C *Combustion and Flame* **39** 133 (1980)
8. Rahn L A, Zych L J, Mattern P L *Opt. Commun.* **30** 249 (1979)
9. Bunkin A F, Koroteev N I *Usp. Fiz. Nauk* **134** 93 (1981) [*Sov. Phys. Usp.* **24** 394 (1981)]
10. Bechtel J H, Chraplyvy A R *Proc. IEEE* **70** 657 (1982)
11. Shaub W M, Nibler J W, Harvey A B *J. Chem. Phys.* **67** 1883 (1977)
12. Gladkov S M, Koroteev N I, in *Itogi Nauki i Tekhniki. Fizicheskie Osnovy Lazernoĭ i Puchkovoĭ Tekhnologii* (Eds N I Koroteev, V Ya Panchenko) (Advances in Science and Technology. Physical Fundamentals of Laser and Beam Technology) Vol. 2 (Moscow: VINITI, 1988) p. 4
13. Bornemann T et al. *Appl. Phys. B* **51** 307 (1990)
14. Gladkov S M et al. *Kvantovaya Elektron.* **18** 727 (1991)
15. Brodnikovskiĭ A M et al. *Pis'ma Zh. Tekh. Fiz.* **8** 497 (1982) [*Sov. Tech. Phys. Lett.* **8** 216 (1982)]
16. Beiting E J *Appl. Opt.* **24** 3010 (1985)
17. Gladkov S M, Koroteev N I *Usp. Fiz. Nauk* **160** 105 (1990) [*Sov. Phys. Usp.* **33** 554 (1990)]
18. Gladkov S M et al. *Izv. Akad. Nauk SSSR, Ser. Fiz.* **52** (2) 217 (1988)
19. Alessandretti G C, Violino P *J. Phys. D* **16** 1583 (1983)
20. Eckbreth A C, Anderson T J, Dobbs G M *Appl. Phys. B* **45** 215 (1988)
21. Lueckerath R et al. *Chemtronics* **2** 199 (1987)
22. Zheltikov A M et al. *Izv. Ross. Akad. Nauk, Ser. Fiz.* **56** (8) 66 (1992) [*Bull. Russ. Acad. Sci. Phys.* **56** 1170 (1992)]
23. Mann B A, White R F, Morrison R J S *Appl. Opt.* **35** 475 (1996)
24. Fedotov A B et al. *Nuovo Cimento D* **14** 1003 (1992)
25. Zheltikov A M et al. *Izv. Ross. Akad. Nauk, Ser. Fiz.* **60** (3) 78 (1996)
26. Sidorov-Biryukov D A et al. *Laser Phys.* **6** 456 (1996)
27. Butylkin V S et al. *Rezonansnye Vzaimodeĭstviya Sveta s Veshchestvom* (Resonant Light–Matter Interactions) (Moscow: Nauka, 1977)
28. Delone N B, Kraĭnov V P *Osnovy Nelineĭnoĭ Optiki Atomarnykh Gazov* (Fundamentals of Nonlinear Optics of Atomic Gases) (Moscow: Nauka, 1986) [Translated into English (New York: Wiley, 1988)]
29. Bakhramov S A, Tartakovskiĭ G Kh, Khabibullaev P K *Nelineĭnye Rezonansnye Protsessy i Preobrazovateli Chastoty v Gazakh* (Nonlinear Resonant Processes and Frequency Converters in Gases) (Tashkent: FAN, 1981)
30. Arkhipkin V G, Popov A K *Nelineĭnoe Preobrazovanie Sveta v Gazakh* (Nonlinear Light Conversion in Gases) (Novosibirsk: Nauka, 1987)
31. Koroteev N I *Vestn. Mosk. Univ. Fiz. Astron.* (6) 6 (1996)
32. Akhmanov S A et al. *Zh. Eksp. Teor. Fiz.* **74** 1272 (1978) [*Sov. Phys. JETP* **47** 667 (1978)]
33. Akhmanov S A, Koroteev N I *Usp. Fiz. Nauk* **123** 405 (1977) [*Sov. Phys. Usp.* **20** 899 (1977)]
34. Ewart P, Snowdon P, Magnusson I *Opt. Lett.* **14** 563 (1989)
35. Akimov D A et al. *Kvantovaya Elektron.* **24** 1154 (1997)
36. Gladkov S M et al. *Pis'ma Zh. Tekh. Fiz.* **14** 1399 (1988) [*Sov. Tech. Phys. Lett.* **14** 610 (1988)]
37. Fedotov A B et al. *J. Opt. Soc. Am. B* **8** 363 (1991)
38. Zheltikov A M, Koroteev N I, Fedotov A B *Opt. Spektrosk.* **72** 971 (1992) [*Opt. Spectrosc.* **72** 527 (1992)]

39. Fedotov A B, Koroteev N I, Zheltikov A M *Laser Applications* (Proc. SPIE, Vol. 2097, Ed. A A Mak) (Bellingham, WA: SPIE, 1993) p. 308
40. Kubodera S et al. *Phys. Rev. A* **48** 4576 (1993)
41. Zheltikov A M, Koroteev N I, Fedotov A B *Laser Phys.* **4** 569 (1994)
42. Fedotov A B, Koroteev N I, Zheltikov A M *Laser Phys.* **5** 835 (1995)
43. Theobald W et al. *Opt. Commun.* **120** 177 (1995)
44. von der Linde D et al. *Phys. Rev. A* **52** R25 (1995)
45. Rebane A K et al. *Kvantovaya Elektron.* **23** 291 (1996) [*Quantum Electron.* **26** 283 (1996)]
46. Fedotov A B et al. *Laser Phys.* **6** 427 (1996)
47. Fedotov A B et al. *Opt. Commun.* **133** 587 (1997)
48. Backus S et al. *Opt. Lett.* **21** 665 (1996)
49. Tarasevitch A, Orisch A, von der Linde D, in *XVI Int. Conference on Coherent and Nonlinear Optics* (ICCNO '98), *Technical Digest: Moscow, 1998* (Moscow: Moscow State Univ., 1998) p. 323
50. Askar'yan G A *Pis'ma Zh. Eksp. Teor. Fiz.* **4** 400 (1966) [*JETP Lett.* **4** 270 (1966)]
51. Gladkov S M et al. *Pis'ma Zh. Eksp. Teor. Fiz.* **43** 227 (1986) [*JETP Lett.* **43** 287 (1986)]
52. Koroteev N I, Zheltikov A M, in *XIV European CARS Workshop* (Madrid: Inst. Struct. Mater., 1995) p. A3
53. Koroteev N I *Usp. Fiz. Nauk* **152** 493 (1987) [*Sov. Phys. Usp.* **30** 628 (1987)]
54. Abrams R L, Lind R C *Opt. Lett.* **2** 94 (1978)
55. Fisher R A (Ed.) *Optical Phase Conjugation* (New York: Academic Press, 1983)
56. Ewart P, O'Leary S V *J. Phys. B* **15** 3669 (1982)
57. Pender J, Hesselink L *Opt. Lett.* **10** 264 (1985)
58. Ewart P, O'Leary S V *Opt. Lett.* **11** 279 (1986)
59. Dreier T, Rakestraw D J *Appl. Phys. B* **50** 479 (1990)
60. Germann G J, Rakestraw D J *Science* **264** 1750 (1994)
61. Fantoni R et al. *Chem. Phys. Lett.* **259** 342 (1996)
62. Dreier T, Rakestraw D J *Opt. Lett.* **15** 72 (1990)
63. Yip B, Danehy P M, Hanson R K *Opt. Lett.* **17** 751 (1992)
64. Smith A P, Astill A G *Appl. Phys. B* **58** 459 (1994)
65. Klamminger A et al. *Appl. Phys. B* **61** 311 (1995)
66. Kaminski C F, Hughes I G, Ewart P *J. Chem. Phys.* **106** 5324 (1997)
67. Butcher P N, Cotter D *The Elements of Nonlinear Optics* (Cambridge: Cambridge University Press, 1990)
68. Meacher D R et al. *Phys. Rev. A* **42** 3018 (1990)
69. Ewart P, Snowdon P *Opt. Lett.* **15** 1403 (1990)
70. Rakestraw D J, Farrow R L, Dreier T *Opt. Lett.* **15** 709 (1990)
71. Ewart P, Kaczmarek M *Appl. Opt.* **30** 3996 (1991)
72. Nyholm K, Fritzon R, Alden M *Appl. Phys. B* **59** 37 (1994)
73. Ljungberg P, Axner O *Appl. Phys. B* **59** 53 (1994)
74. Ljungberg P, Axner O *Appl. Opt.* **34** 527 (1995)
75. Ewart P, O'Leary S V *J. Phys. B* **17** 4595 (1984)
76. Bratfalean R, Ewart P *J. Mod. Opt.* **43** 2523 (1996)
77. Konz K E, Marowsky G, Rubahn H-G *Opt. Commun.* **134** 75 (1997)
78. Kaminski C F, Loefstedt B, Alden M, in *XV European CARS Workshop* (ECW '96) (Sheffield: Univ. Sheffield, 1996) p. A22
79. Ewart P, Smith P G R, Williams R B *Appl. Opt.* **36** 5959 (1997)
80. Maker P D, Terhune R W *Phys. Rev.* **137** A801 (1965)
81. Yablonovitch E, Flytzanis C, Bloembergen N *Phys. Rev. Lett.* **29** 865 (1972); Druet S A J, Taran J-P E *Prog. Quantum Electron.* **7** 1 (1981)
82. Akhmanov S A et al. *Pis'ma Zh. Eksp. Teor. Fiz.* **15** 600 (1972) [*JETP Lett.* **15** 425 (1972)]
83. Roh W B, Schreiber P W, Taran J P E *Appl. Phys. Lett.* **29** 174 (1976)
84. Smirnov V V, Fabelinskiĭ V I *Pis'ma Zh. Eksp. Teor. Fiz.* **28** 461 (1978) [*JETP Lett.* **28** 427 (1978)]
85. Osin M N et al. *Zh. Tekh. Fiz.* **51** 106 (1981) [*Sov. Phys. Tech. Phys.* **26** 58 (1981)]
86. Murphy D V, Chang R K *Opt. Lett.* **6** 233 (1981)
87. Bunkin A F, Ivanov S G, Koroteev N I *Pis'ma Zh. Tekh. Fiz.* **3** 450 (1977)
88. Aliev M R, Kozlov D N, Smirnov V V *Pis'ma Zh. Eksp. Teor. Fiz.* **26** 31 (1977) [*JETP Lett.* **26** 27 (1977)]
89. Fabelinsky V I et al. *Opt. Commun.* **20** 389 (1977); Kiefer W *J. Molec. Structure* **59** 305 (1980)
90. Azizbekyan G V et al. *Kvantovaya Elektron.* **4** 1911 (1977) [*Sov. J. Quantum Electron.* **7** 1086 (1977)]
91. Akhmanov S A et al. *Pis'ma Zh. Eksp. Teor. Fiz.* **26** 603 (1977) [*JETP Lett.* **26** 453 (1977)]
92. Valyanskiĭ S I et al. *Tr. Inst. Obshch. Fiz. Akad. Nauk SSSR* **2** 117 (1986)
93. D'yakov Yu E et al. *Zh. Eksp. Teor. Fiz.* **84** 2013 (1983) [*Sov. Phys. JETP* **57** 1172 (1983)]
94. Akhmanov S A et al. *J. Opt. Soc. Am. B* **2** 640 (1985)
95. Akhmanov S A et al. *Opt. Spektrosk.* **64** 503 (1988) [*Opt. Spectrosc.* **64** 301 (1988)]
96. Pichler G et al. *Nuovo Cimento D* **14** 1065 (1992)
97. Brodnikovskiĭ A M et al. *Zh. Eksp. Teor. Fiz.* **84** 1664 (1983) [*Sov. Phys. JETP* **57** 971 (1983)]
98. Gladkov S M et al. *Opt. Spektrosk.* **65** 249 (1988) [*Opt. Spectrosc.* **65** 149 (1988)]
99. Kung A H *Appl. Phys. Lett.* **25** 653 (1974)
100. Hilbig R, Wallenstein R *Appl. Opt.* **21** 913 (1982)
101. Freeman R R et al. *Appl. Phys. Lett.* **33** 739 (1978)
102. Corney A, Gardner K *J. Phys. B* **11** 2037 (1978)
103. Bunkin S B et al. *Opt. Spektrosk.* **66** 1182 (1989) [*Opt. Spectrosc.* **66** 690 (1989)]
104. Murphy D V et al. *Opt. Lett.* **4** 167 (1979)
105. Snow J B, Zheng J, Chang R K *Opt. Lett.* **8** 599 (1983)
106. Jonuscheit J et al. *Opt. Lett.* **21** 1532 (1996)
107. Eckbreth A C, Anderson T J *Appl. Opt.* **24** 2731 (1985)
108. Eckbreth A C, Anderson T J *Opt. Lett.* **11** 496 (1986)
109. Aldén M, Bengtsson P-E, Edner H *Appl. Opt.* **25** 4493 (1986)
110. Laufer G, Miles R B *Opt. Commun.* **28** 250 (1979)
111. Laufer G, Miles R B, Santavicca D *Opt. Commun.* **31** 242 (1979)
112. Buldakov M A et al. *Kvantovaya Elektron.* **11** 405 (1984) [*Sov. J. Quantum Electron.* **14** 278 (1984)]
113. Evsin O A et al. *Kvantovaya Elektron.* **22** 295 (1995) [*Quantum Electron.* **25** 278 (1995)]
114. Koroteev N I et al., in *ICONO '98: Laser Spectroscopy and Optical Diagnostics* (Proc. SPIE, Vol. 3732, Eds A Y Chikishev, V N Zadkov, A M Zheltikov) (Bellingham, WA: SPIE, 1999)
115. Gladkov S M et al. *Kvantovaya Elektron.* **14** 1086 (1987) [*Sov. J. Quantum Electron.* **17** 687 (1987)]
116. Gladkov S M et al. *Kvantovaya Elektron.* **16** 1430 (1989) [*Sov. J. Quantum Electron.* **19** 923 (1989)]
117. Gladkov S M et al. *Pis'ma Zh. Tekh. Fiz.* **15** (13) 24 (1989) [*Sov. Tech. Phys. Lett.* **15** 505 (1989)]
118. Koroteev N I et al. *Laser Phys.* **7** 45 (1997)
119. Koroteev N I et al. *Bull. Russ. Acad. Sci. Phys. Suppl. Phys. Vibr.* **60** 149 (1996)
120. Fedotov A B et al. *Laser Phys.* **8** 570 (1998)
121. Koroteev N I, Zheltikov A M *Mol. Cryst. Liq. Cryst. Sci. Technol. Sec. B: Nonlinear Optics* **3** 319 (1992)
122. Akimov D A et al. *Opt. Commun.* **140** 259 (1997)
123. Fedotov A B et al. *J. Nonlinear Optical Phys. Mater.* **6** 387 (1997)
124. Shkolnikov P L, Kaplan A E, Lago A *Opt. Lett.* **18** 1700 (1993)
125. Zheltikov A M, Koroteev N I, Naumov A N *Kvantovaya Elektron.* **21** 1189 (1994) [*Quantum Electron.* **24** 1102 (1994)]
126. Koroteev N I, Naumov A N, Zheltikov A M *Laser Phys.* **4** 1160 (1994)
127. Naumov A N, Koroteev N I, Zheltikov A M *Laser Phys.* **5** 965 (1995)
128. Gladkov S M, Zheltikov S M, Il'yasov O S, in *Proc. XX All-Union Congress on Spectroscopy*, Kiev, 1988 Pt. 1 (Kiev: Naukova Dumka, 1988) p. 101
129. Akimov D A et al. *Laser Phys.* **7** 99 (1997)
130. Miles R B, Harris S E *IEEE J. Quantum Electron.* **QE-9** 470 (1973)
131. McPherson A et al. *J. Opt. Soc. Am. B* **4** 595 (1987)
132. Ferray M et al. *J. Phys. B* **21** L31 (1988)
133. Li X F et al. *Phys. Rev. A* **39** 5751 (1989)
134. Balcou Ph et al. *J. Phys. B* **25** 4467 (1992)
135. Sarukura N et al. *Phys. Rev. A* **43** 1669 (1991)
136. Macklin J J, Kmetec J D, Gordon C L *Phys. Rev. Lett.* **70** 766 (1993)
137. Kondo K et al. *Phys. Rev. A* **47** 2480 (1993)
138. Wahlstrom C-G et al. *Phys. Rev. A* **48** 4709 (1993)
139. Mittleman D M et al. *J. Opt. Soc. Am. B* **13** 170 (1996)
140. Spielmann Ch et al. *Science* **278** 661 (1997)
141. Spielmann Ch et al., in *Conference on Lasers and Electro-Optics* (*CLEO '98*), *Technical Digest, 1998 OSA Technical Digest Series*, Vol. 6 (Washington, DC: Opt. Soc. Am., 1998) p. 81

142. Marcatili E A J, Schmeltzer R A *Bell Syst. Tech. J.* **43** 1783 (1964)
143. Miles R B, Laufer G, Bjorklund G C *Appl. Phys. Lett.* **30** 417 (1977)
144. Nisoli M, De Silvestri S, Svelto O *Appl. Phys. Lett.* **68** 2793 (1996)
145. Nisoli M et al. *Opt. Lett.* **22** 522 (1997)
146. Sartania S et al. *Opt. Lett.* **22** 1562 (1997)
147. Durfee C G et al. *Opt. Lett.* **22** 1565 (1997)
148. Koroteev N I, Zheltikov A M *Laser Phys.* **8** 512 (1998)
149. Koroteev N I, Zheltikov A M *Appl. Phys. B* **67** 53 (1998)
150. Tamaki Y, Midorikawa K, Obara M *Appl. Phys. B* **67** 59 (1998)
151. Durfee C G et al., in *Int. Quantum Electronic Conference* (*IQEC '98), Postdeadline Papers* (Washington, DC: Opt. Soc. Am., 1998) p. QPD5
152. Akimov D A et al. *Opt. Lett.* **24** 478 (1999)
153. Ward J F, New G H C *Phys. Rev.* **185** 57 (1969)
154. Bjorklund G C *IEEE J. Quantum Electron.* **QE-11** 287 (1975)
155. Koroteev N I, Naumov A N, Zheltikov A M *Laser Phys.* **4** 1160 (1994)
156. Zheltikov A M et al. *Laser Phys.* **6** 49 (1996)
157. Sedov L L *Metody Podobiya i Razmernosti v Mekhanike* (Methods of Similarity and Dimensions in Mechanics) (Moscow: Nauka, 1981)
158. Korobeĭnikov V P, Mel'nikova N S, Ryazanov E V *Teoriya Tochechnogo Vzryva* (Theory of Point Explosion) (Moscow: Fizmatgiz, 1961)
159. Ostrovskaya G V, Zaĭdel' A N *Usp. Fiz. Nauk* **111** 579 (1973) [*Sov. Phys. Usp.* **16** 834 (1974)]
160. Zheltikov A M et al., in *Int. Quantum Electronic Conference* (IQEC '98), *1998 OSA Technical Digest Series* Vol. 7 (Washington, DC: Opt. Soc. Am., 1998) p. 147
161. Akimov D A et al., in *ICONO '98: Laser Spectroscopy and Optical Diagnostics* (Proc. SPIE, Vol. 3732, Eds A Y Chikishev, V N Zadkov, A M Zheltikov) (Bellingham, WA: SPIE, 1999)
162. Kröll S et al. *Appl. Opt.* **26** 1068 (1987)
163. Snelling D R, Sawchuk R A, Parameswaran T *Appl. Opt.* **33** 8295 (1994)
164. Ewart P *Opt. Commun.* **55** 124 (1985)
165. Snowdon P, Skippon S M, Ewart P *Appl. Opt.* **30** 1008 (1991)
166. Kaminski C F, Ewart P *Appl. Opt.* **36** 731 (1997)
167. Kaminski C F, Ewart P *Appl. Phys. B* **64** 103 (1997)
168. Gladkov S M, Zheltikov A M, Koroteev N I, in *Itogi Nauki i Tekhniki. Sovremennye Problemy Lazernoĭ Fiziki* (Ed. S A Akhmanov) (Advances in Science and Technology. Modern Problems of Laser Physics) Vol. 4 (Moscow: VINITI, 1991) p. 126
169. Czarnetzki U, Dobele H F *Phys. Rev. A* **44** 7530 (1991)
170. Schulz-von der Gathen V et al. *IEEE J. Quantum Electron.* **QE-26** 739 (1990)
171. Wellegehausen B et al., in *Conference on Lasers and Electro-Optics Europe, Technical Digest* (Hamburg: Hamburg Univ., 1996) p. 331
172. Payne D S et al., in *XV European CARS Workshop* (ECW '96) (Sheffield: Univ. Sheffield, 1996) p. A20
173. Fedotov A B et al. *Bull. Russ. Acad. Sci. Phys. Suppl. Phys. Vibr.* **58** 115 (1994)
174. Biberman L M, Vorob'ev V S, Yakubov I T *Kinetika Neravnovesnoĭ Nizkotemperaturnoĭ Plazmy* (Kinetics of Nonequilibrium Low-Temperature Plasmas) (Moscow: Nauka, 1982) [Translated into English (New York: Consultants Bureau, 1987)]
175. Bokhan P A *Kvantovaya Elektron.* **13** 1837 (1986) [*Sov. J. Quantum Electron.* **16** 1207 (1986)]
176. Astadzhov D N et al. *Kvantovaya Elektron.* **14** 396 (1987) [*Sov. J. Quantum Electron.* **17** 245 (1987)]
177. Astadzhov D N et al. *Tr. Fiz. Inst. Akad. Nauk SSSR* **181** 122 (1987)
178. Batenin V M et al., Preprint No. 5-210 (Moscow: Inst. High Temperatures, USSR Acad. Sci., 1985)
179. Oudar J-L, Smith R W, Shen Y R *Appl. Phys. Lett.* **34** 758 (1979)
180. Vigasina M F et al. *Dokl. Akad. Nauk SSSR* **283** 1394 (1985)
181. Koroteev N I, Endemann M, Byer R L *Phys. Rev. Lett.* **43** 398 (1979)
182. Lotem H, Lynch R T (Jr.), Bloembergen N *Phys. Rev. A* **14** 1748 (1976)
183. Aslanyan L S, Bunkin A F, Koroteev N I *Pis'ma Zh. Tekh. Fiz.* **4** 1177 (1978) [*Sov. Tech. Phys. Lett.* **4** 473 (1978)]
184. Ivanov A A et al. *Opt. Spektrosk.* **66** 1046 (1989) [*Opt. Spectrosc.* **66** 611 (1989)]
185. Levenson M D, Bloembergen N *Phys. Rev. B* **10** 4447 (1974)
186. Levenson M D, Bloembergen N *J. Chem. Phys.* **60** 1323 (1974)
187. Bunkin A F, Ivanov S G, Koroteev N I *Dokl. Akad. Nauk SSSR* **233** 338 (1977) [*Sov. Phys. Dokl.* **22** 146 (1977)]
188. Akhmanov S A et al. *Pis'ma Zh. Eksp. Teor. Fiz.* **25** 244 (1977) [*JETP Lett.* **25** 416 (1977)]
189. Akhmanov S A et al. *Pis'ma Zh. Eksp. Teor. Fiz.* **25** 444 (1977) [*JETP Lett.* **25** 416 (1977)]
190. Oudar J-L, Shen Y R *Phys. Rev. A* **22** 1141 (1980)
191. Aslanyan L S, Bunkin A F, Koroteev N I *Opt. Spektrosk.* **46** 165 (1978)
192. Nestor J R *J. Raman Spectrosc.* **7** 90 (1978)
193. Ferrante G, Koroteev N I, Zheltikov A M *Laser Phys.* **6** 1095 (1996)
194. Zheltikov A M, Koroteev N I, Sidorov-Biryukov D A *Kvantovaya Elektron.* **21** 509 (1994) [*Quantum Electron.* **24** 467 (1994)]
195. Koroteev N I, Shumaĭ I L *Fizika Moshchnogo Lazernogo Izlucheniya* (Physics of High-Power Laser Radiation) (Moscow: Nauka, 1991)
196. Fano U *Phys. Rev.* **124** 1866 (1961)
197. Fano U, Cooper J W *Phys. Rev.* **137** A1364 (1965)
198. Fano U *Phys. Rev. A* **2** 353 (1970)
199. Geller Yu I, Popov A K *Lazernoe Indutsirovanie Nelineĭnykh Rezonansov v Sploshnykh Spektrakh* (Laser Induction of Nonlinear Resonances in the Continuous Spectrum) (Novosibirsk: Nauka, 1981)
200. Armstrong J A, Wynne J J, in *Nonlinear Spectroscopy* (Ed. N Bloembergen) (Amsterdam: North-Holland, 1977) p. 152
201. Bekov G I et al. *Pis'ma Zh. Eksp. Teor. Fiz.* **28** 308 (1978) [*JETP Lett.* **28** 283 (1978)]
202. Armstrong J A, Wynne J J *Phys. Rev. Lett.* **33** 1183 (1974)
203. Nittoh R et al. *J. Phys. B* **27** 1955 (1994)
204. Bekov G I et al. *Opt. Commun.* **35** 194 (1980)
205. Bekov G I et al. *Zh. Eksp. Teor. Fiz.* **80** 866 (1981) [*Sov. Phys. JETP* **53** 441 (1981)]
206. Pavlov L I et al. *Phys. Lett. A* **89** 441 (1982)
207. Dimov S S et al. *Appl. Phys. B* **30** 35 (1983)
208. Elizarov A Yu, Cherepkov N A *Zh. Eksp. Teor. Fiz.* **96** 1224 (1989) [*Sov. Phys. JETP* **69** 695 (1989)]
209. Bobashev S V et al. *Laser Phys.* **3** 751 (1993)
210. Bobashev S V et al. *Zh. Eksp. Teor. Fiz.* **106** 90 (1994) [*JETP* **79** 47 (1994)]
211. Elizarov A Yu *Pis'ma Zh. Eksp. Teor. Fiz.* **62** 23 (1995) [*JETP Lett.* **62** 23 (1995)]
212. Zheltikov A M, Il'yasov O S, Koroteev N I *Pis'ma Zh. Eksp. Teor. Fiz.* **54** 143 (1991) [*JETP Lett.* **54** 139 (1991)]
213. Bloembergen N, Lotem H, Lynch R T *Indian J. Pure Appl. Phys.* **16** 151 (1978)
214. Akimov D A et al. *Laser Phys.* **7** 755 (1997)
215. Sidorov-Biryukov D A, Zheltikov A M, Koroteev N I *Kvantovaya Elektron.* **23** 101 (1996) [*Quantum Electron.* **26** 97 (1996)]
216. Antcliff R R, Jarrett O, Jr. *Rev. Sci. Instrum.* **58** 2075 (1987)
217. Miles R B et al. *AIAA J.* **31** 447 (1993)
218. Ishimaru A *Wave Propagation and Scattering in Random Media* (New York: Academic Press, 1978)
219. Natterer F *The Mathematics of Computerized Tomography* (Stuttgart: B.G. Teubner, 1986)
220. Tikhonov A N, Arsenin V Ya, Timonov A A *Matematicheskie Zadachi Komp'yuternoĭ Tomografii* (Mathematical Problems of Computer Tomography) (Moscow: Nauka, 1987)
221. *Medical Optical Tomography: Functional Imaging and Monitoring* (SPIE Institutes for Advanced Optical Technologies, Vol. IS11, Eds G Muller et al.) (Bellingham, WA: SPIE, 1993)
222. Minerbo G N et al. *Appl. Opt.* **19** 1723 (1980)
223. Chen Y W et al. *J. Appl. Phys.* **68** 1483 (1990)
224. Russanov E V, Vishnyakov G N, in *Analytical Methods for Optical Tomography* (Proc. SPIE, Vol. 1843, Ed. G G Levin) (Bellingham, WA: SPIE, 1992) p. 83
225. Balandin A L et al., in *Analytical Methods for Optical Tomography* (Proc. SPIE, Vol. 1843, Ed. G G Levin) (Bellingham, WA: SPIE, 1992) p. 68
226. Koroteev N I, Naumov A N, Zheltikov A M, in *7th Int. Conference Laser Applications in Life Sciences* (Bratislava: Int. Laser Center, 1998) p. P2-18
227. Duncan M D, Reintjes J, Manuccia T J *Opt. Lett.* **7** 350 (1982)
228. Eckbreth A C *Appl. Phys. Lett.* **32** 421 (1978)